Title
COLLECTIVE MODEL DESCRIPTION OF TRANSITIONAL ODD-A NUCLEI. I. THE TRIAXIAL-ROTOR-PLUS-PARTICLE MODEL

Author
Meyer-ter-Vehn, J.

Publication Date
1975

Submitted to Nuclear Physics A

LBL-3458
Preprint

COLLECTIVE MODEL DESCRIPTION OF TRANSITIONAL ODD-A NUCLEI
I. THE TRIAXIAL-ROTOR-PLUS-PARTICLE MODEL

J. Meyer-ter-Vehn

January 1975

Prepared for the U. S. Atomic Energy Commission
under Contract W-7405-ENG-48

DISCLAIMER

COLLECTIVE MODEL DESCRIPTION OF TRANSITIONAL ODD-A NUCLEI

I. THE TRIAXIAL-ROTOR-PLUS-PARTICLE MODEL*

J. Meyer-ter-Vehn†

Lawrence Berkeley Laboratory
University of California
Berkeley, California 94720

---

*Work performed under the auspices of the U. S. Atomic Energy Commission and supported in part by the Deutsche Forschungsgemeinschaft.

†On leave of absence from Physik-Department, Technische Universität München, München, West Germany.

ABSTRACT

The energy spectrum of an odd nucleon coupled to a triaxial rotating core has been calculated as a function of the deformation β, the asymmetry γ and the Fermi energy λ_F. Results are presented in a series of plots with the odd nucleon restricted to a single j-shell and the parameters covering the area which is of most interest for transitional odd-A nuclei in the A = 135 and the A = 190 mass region. The results apply to unique-parity spectra which are based either on particle or hole states in a j = 11/2 shell, but hold also for j = 9/2 and j = 13/2. In addition, results on moments and transition probabilities are given. The quasi-particle-rotor Hamiltonian is derived with special emphasis on the particle-hole symmetry. The analytic solution for the even triaxial rotor at $\gamma = 30°$ is given. Concerning the odd-A spectrum, characteristics which can be tested experimentally are discussed, and a qualitative physical interpretation is given. In particular, band structures in the triaxial region and their approximate classification are pointed out.

1. INTRODUCTION

One of the new results obtained from heavy-ion experiments is the excitation of high-spin rotation-like bands in nuclei well beyond the established rotational regions. These results suggest that the concept of collective nuclear rotation has a wider range of validity than assumed in the past and is also applicable in the transitional regions between rotational and closed-shell nuclei. It has been shown recently by Stephens that the yrast bands of a number of transitional odd-A nuclei can be understood in terms of an odd nucleon in a high-j shell coupled to a rotating core.[1]) One of the objectives of the present work is to show that this concept holds more generally for whole families of unique-parity states including high-spin *and* low-spin states.

The unique parity states in heavy odd-A nuclei, on which the present investigation is focussed, are a very interesting group of states, since they represent a "simple case" in otherwise more complicated spectra. The configuration of the odd nucleon in these states consists of an almost pure high-j shell ($h_{11/2}$, $i_{13/2}$, etc.) which does not mix with neighboring shells due to its opposite parity. The family of states belonging to such a j-shell is easily identified in the experimental spectra, since their members decay predominantly within the family. In some favored cases, rather complete families of unique parity states are now known with high-spin states obtained from heavy-ion experiments and low-spin states observed in β-decay.

Because of the pure configuration of the odd nucleon, the energy spectrum of a family of unique-parity states gives rather direct information on the shape and the collective motion of the core. The main point of

the present work will be that the odd-A spectra are particularly sensitive to *triaxial* shapes and that certain families of unique-parity states contain detailed evidence for triaxial nuclear deformations. Because of the larger level density of odd-A nuclei at low energy, this evidence goes far beyond what can be obtained from even nuclei. Some of the results have already been reported.[2]) In the present publication, a more complete account of this work is given.

The shapes of transitional nuclei are known to be rather soft. They fluctuate about average shapes which are of moderate deformation ($0.1 < \beta < 0.2$) and triaxial ($0° < \gamma < 60°$). The theory of the collective motion of the nuclear surface and the coupling of an odd nucleon to this motion has been formulated by Bohr and Mottelson.[3]) A complete dynamical solution of their equations is fairly complicated already for even nuclei[4,5]) and will be more cumbersome for the odd-A case. In the present work, therefore, the Davydov approximation[6]) is used which fixes the collective wavefunction at its average values, assuming a rigid triaxial shape. This is certainly a serious limitation which needs some comments.

The use of a fixed shape affects the odd-A solution at two points: (i) at the energies and wavefunctions of the core, and (ii) at the coupling of the odd nucleon to the core. Concerning the first point, it should be recalled that, on the one hand, the spectrum of a rigid triaxial rotor approximately reproduces the lowest excited states of even transitional nuclei, e.g., in the A = 190 and A = 135 mass regions. In particular, it accounts for the low-lying second 2^+ states which are characteristic for triaxial shapes. On the other hand, there are systematic deviations which reflect the softness of these nuclei.

Especially, one observes an overall compression of the experimental spectra as compared with that of a rigid triaxial rotor and, in the calculated odd-A spectra, this deviation will, of course, show up in a parallel way.†

It should be noticed, however, that the second point concerning the particle-core coupling is the more important factor with respect to the odd-A spectrum because it determines the level order, and, at this point, the approximation of fixed triaxial shapes turns out to be well supported by the comparison with experiment. The odd-A spectrum changes drastically when going from prolate-type ($0° < \gamma < 30°$) to oblate-type ($30° < \gamma < 60°$) shapes. Such a transition is observed in the A = 190 mass region and is well described assuming rigid triaxial shapes. In fact, it will be the surprising result of the present investigation that rather complex families of unique-parity states can be reproduced with fixed β and γ values derived from neighboring even nuclei and that, apparently, the core parameters are not much influenced by adding the odd nucleon. Based on this observation, it will be concluded that a number of transitional nuclei are less soft than expected from existing theoretical calculations of potential energy surfaces.

There exists previous work on odd-A triaxial rotors. In some of the publications,[7]) the adiabatic approximation is applied which considers the odd nucleon to be in a definite single-particle state. This restriction

---

†One could use the empirical core energies in the odd-A calculation to reduce this discrepancy. In the present work, the solution of the pure triaxial model is preferred since it allows a more general presentation.

is certainly inadequate for weakly deformed nuclei where the coupling of the odd nucleon to the intrinsic shape is relatively small and the Coriolis mixing large. It is therefore important to take at least one complete j-shell for the single-particle configuration space so that the odd nucleon is free to orient its angular momentum relative to the core or to move uncorrelated to the intrinsic shape. It is this point which insures that the model contains the weak-coupling limit as well as the strong-coupling limit and is able to describe the various intermediate regions. The first calculation of this type has been done by Pashkevich and Sardaryan[8]). The present calculation is basically the same, but treats the odd nucleon as a BCS-quasiparticle, thus accounting for the Pauli principle in partially filled shells. Only one-quasiparticle states are considered. This limits the applicability of the model to low-excited states below 2Δ, where Δ denotes the pairing gap.

The present report is divided into two parts. Part I, given in this paper, presents the basic equations and symmetries of the model and provides a general survey over the model solution. Special emphasis is put on the physical interpretation. In Part II, the model calculation will be compared with some representative experimental cases in the $A = 135$ and $A = 190$ mass region. The question of softness and how the present result relates to other work on transitional nuclei will be discussed there. For convenience, a Table of Contents of the following chapters of Part I is given here:

2. THE THEORETICAL MODEL

2.1. Single-particle and single-hole states

The model investigated in this paper consists of an odd nucleon coupled to a rotating triaxial core. The odd nucleon is considered as a quasiparticle that represents either a particle or a hole or a superposition of both. Its configuration space will be restricted to a single j-shell which is either filled or unfilled or partly filled by core particles. The quasiparticle will be described within the BCS approximation. The basic equations (2.6), (2.11), and (2.15) are written in a (2×2)-matrix notation which accounts in an explicit way for the particle and the hole equation and the coupling of both by the pairing interaction. The particle-hole symmetry (2.22) of the model can be conveniently discussed in this presentation.

Particle and hole states can be expressed in the form[9])

$$|j\Omega\rangle = a^{\dagger}_{j\Omega} \, |\hat{0}\rangle \quad , \tag{2.1a}$$

and

$$|j^{-1}\Omega\rangle = (-)^{j+\Omega} \, a_{j-\Omega} \, |\hat{0}\rangle \quad , \tag{2.1b}$$

respectively, where $a^{\dagger}_{j\Omega}$ and $a_{j\Omega}$ are creation and annihilation operators for a particle in the j-shell, and $|\hat{0}\rangle$ denotes the ground-state of an even nucleus with mass A. The energy of the states in the

spherical j-shell are conveniently defined relative to the Fermi energy λ_F. One has $(\varepsilon_j - \lambda_F)$ for particle states, and $(\lambda_F - \varepsilon_j)$ for hole states. The matrix elements of a single-particle operator F for particle and hole states are related by the particle-hole conjugation[9])

$$\langle j^{-1}\Omega_1 |F| j^{-1}\Omega_2 \rangle = -c \langle j\Omega_1 |F| j\Omega_2 \rangle + \langle 0 |F| \hat{0} \rangle \delta_{\Omega_1\Omega_2} , \qquad (2.2)$$

where c is determined by the symmetry of F under the time reversal

$$T F T^{-1} = c F . \qquad (2.3)$$

For the deformation potential V_p of the core see [Eq. (2.7)], which splits the degenerate levels of the j-shell, one obtains

$$\langle j^{-1}\Omega_1 |V_p| j^{-1}\Omega_2 \rangle = - \langle j\Omega_1 |V_p| j\Omega_2 \rangle + \langle \hat{0}|V_p|\hat{0} \rangle \delta_{\Omega_1\Omega_2} . \qquad (2.4)$$

Beside the deformation interaction V_p, the pairing interaction is taken into account by the pairing potential $\hat{\Delta}$ which couples particle and hole states

$$\langle j\Omega_1 |\hat{\Delta}| j^{-1}\Omega_2 \rangle = \langle j^{-1}\Omega_1 |\hat{\Delta}^\dagger| j\Omega_2 \rangle = \Delta\delta_{\Omega_1\Omega_2} . \qquad (2.5)$$

Here, Δ is the usual gap parameter.

In the present work, the core is treated as a collective rotor. The potentials V_p and Δ and the inertia parameters in Eq. (2.12), which characterize the core, can be considered as arising from an underlying microscopic theory. Within the present approach, however, they are determined phenomenologically.

2.2. The Quasiparticle-Rotor Hamiltonian

On the basis of relations (2.4) and (2.5), the Hamiltonian of the odd nucleon is obtained in the form

$$\mathcal{H}_p = (\varepsilon_j - \lambda_F) \cdot \begin{pmatrix} 1 & \\ & -1 \end{pmatrix} + V_P \cdot \begin{pmatrix} 1 & \\ & -1 \end{pmatrix} + \Delta \cdot \begin{pmatrix} & 1 \\ 1 & \end{pmatrix} . \quad (2.6)$$

The energy of the spherical shell ε_j is set = 0 in the following. The deformation potential

$$V_p(\beta,\gamma,\theta,\phi) = k(r)\beta \left[\cos\gamma\ Y_{20}(\theta,\phi) + \frac{\sin\gamma}{\sqrt{2}} \left(Y_{22}(\theta,\phi) + Y_{2-2}(\theta,\phi)\right)\right] \quad (2.7)$$

is generated by the ellipsoidal shape of the core with the semi-axes

$$R_\kappa = R_o \left(1 + \sqrt{\frac{5}{4\pi}}\,\beta\cos\left(\gamma - \frac{2\pi}{3}\,\kappa\right)\right) \qquad \kappa = 1,2,3 \ . \quad (2.8)$$

The deformation parameter β and the asymmetry parameter γ determine the shape, $k(r)$ determines the radial dependence of V_p, $Y_{2\mu}$ are spherical harmonics, and R_o is the nuclear radius. The Pauli matrices in Eq. (2.6) refer to the particle and the hole space. The two subspaces are defined explicitly by the vectors

$$|j\Omega\rangle_{s.p.} = \chi_\Omega^{(j)}(\vec{r}) \begin{pmatrix} 1 \\ 0 \end{pmatrix}, \quad (2.9a)$$

$$|j\Omega\rangle_{s.h.} = \chi_\Omega^{(j)}(\vec{r}) \begin{pmatrix} 0 \\ 1 \end{pmatrix}, \quad (2.9b)$$

where $\chi_\Omega^{(j)}(\vec{r})$ is given by

$$\chi_\Omega^{(j)}(\vec{r}) = f(r) \cdot Y_{j\Omega}(\theta,\phi) \ . \quad (2.10)$$

The term $\langle \hat{0}|V_p|\hat{0}\rangle$ of Eq. (2.4) has been omitted in Eq. (2.6), since it can be absorbed into λ_F and a constant term added to $\mathcal{H}_p$.

The rotational Hamiltonian of the core is

$$\mathcal{H}_R = h_R \cdot \begin{pmatrix} 1 & & \\ & & \\ & & 1 \end{pmatrix} , \tag{2.11}$$

where

$$h_R = \sum_{\kappa=1}^{3} \frac{(I_\kappa - j_\kappa)^2}{2\mathcal{J}_\kappa} . \tag{2.12}$$

In Eq. (2.11), it is assumed that

$$_{s.h.}\langle j\Omega_1|\mathcal{H}_R|j\Omega_2\rangle_{s.h.} = {}_{s.p.}\langle j\Omega_1|\mathcal{H}_R|j\Omega_2\rangle_{s.p.} , \tag{2.13}$$

implying that the energy of the rotating core does not depend on whether the odd nucleon is represented by a particle or a hole. In Eq. (2.12) I_κ and j_κ are the components of the total and the single-particle angular momentum, respectively. The three moments-of-inertia are chosen as

$$\mathcal{J}_\kappa = \mathcal{J}_o \cdot \frac{4}{3} \sin^2 (\gamma - \frac{2\pi}{3}\kappa) , \qquad \kappa = 1,2,3 , \tag{2.14}$$

throughout this work, unless stated differently. The dependence of $\mathcal{J}_\kappa$ on the shape asymmetry γ is that of irrotational flow; the overall value $\mathcal{J}_o$ will be adjusted. It coincides with the normal moment-of-inertia of axially symmetric deformed nuclei at $\gamma = 0°$ and $\gamma = 60°$.

2.3. The Symmetries

The total Hamiltonian

$$\mathcal{H} = \mathcal{H}_p + \mathcal{H}_R \tag{2.15}$$

is invariant under 180°-rotations about the intrinsic axes (D_2 symmetry group). These symmetries allow the wavefunction to be written in the form

$$\Psi_{IM,\alpha} = \sqrt{\frac{2I+1}{16\pi^2}} \sum_{K,\Omega,\tau}{}' C^{(I,j,\alpha)}_{K\Omega\tau} \left(D^{(I)}_{MK} \chi^{(j)}_{\Omega\tau} + (-)^{(I-j)} D^{(I)}_{M-K} \chi^{(j)}_{-\Omega\tau} \right) , \tag{2.16}$$

where the summation is restricted to $|K| \leqslant I$, $|\Omega| \leqslant j$, $(K+j)$ even, $(\Omega+j)$ even, and $\tau = \pm 1$; $D^{(I)}_{MK}$ denote rotational D-functions. The index τ distinguishes between particle and hole states, and α labels all states for a certain total angular momentum I.

There are more symmetries in the problem arising from permutations of the intrinsic axes and particle-hole conjugation. The six different ways of labeling the intrinsic axes correspond to six equivalent domains in (β,γ)-space

$$\gamma = \pm \gamma', \pm \gamma' + 120°, \pm \gamma' + 240°$$

with $0° \leqslant \gamma' \leqslant 60°$ and $\beta > 0$. Each domain describes the same set of possible shapes. Table 1 shows the γ-values for which axially symmetric oblate and prolate shapes occur and gives the corresponding symmetry axes. For the potential V_p, which depends on the particular choice of the axes, cyclic permutations give rise to the symmetry relations

$$V_p(\beta,\gamma,\theta_3,\phi_3) = V_p(\beta,\gamma + 120°,\theta_1,\phi_1) = V_p(\beta,\gamma + 240°,\theta_2,\phi_2) , \tag{2.17}$$

where the subscript at θ,ϕ defines the axes to which the polar angles are related. Another symmetry relation derived from Eqs. (2.7) and (2.17)

is

$$V_p(\beta,\gamma,\theta_3,\phi_3) = -V_p(\beta, 60^\circ-\gamma, \theta_2,\phi_2) \quad . \tag{2.18}$$

From this relation and particle-hole conjugation, a basic particle-hole symmetry can be derived. Defining a transformation Γ that transforms the set of parameters β, γ, λ_F, Δ and the axes $\hat{1}$, $\hat{2}$, $\hat{3}$ simultaneously according to

$$\begin{aligned} \Gamma: \quad & (\beta, \gamma, \lambda_F, \Delta) \to (\beta, 60^\circ - \gamma, -\lambda_F, -\Delta) \ , \\ & (\hat{1}, \hat{2}, \hat{3}) \to (\hat{3}, \hat{1}, \hat{2}) \ , \end{aligned} \tag{2.19}$$

one obtains from Eqs. (2.6) and (2.18)

$$\Gamma^\dagger \mathcal{H}_p \Gamma = -\mathcal{H}_p \ , \tag{2.20a}$$

and, applying Γ to Eqs. (2.11), (2.12), and (2.14),

$$\Gamma^\dagger \mathcal{H}_R \Gamma = \mathcal{H}_R \ . \tag{2.20b}$$

On the other hand, particle-hole conjugation yields

$$\sigma_y^\dagger \mathcal{H}_p \sigma_y = -\mathcal{H}_p \ , \tag{2.21a}$$

$$\sigma_y^\dagger \mathcal{H}_R \sigma_y = \mathcal{H}_R \ , \tag{2.21b}$$

using the Pauli matrix $\sigma_y = \begin{pmatrix} & i \\ -i & \end{pmatrix}$. The combination of Eqs. (2.20) and (2.21) leads to the important particle-hole symmetry of the total Hamiltonian (2.15)

$$(\sigma_y \Gamma)^\dagger \mathcal{H} (\sigma_y \Gamma) = \mathcal{H} \quad . \tag{2.22}$$

This symmetry, expressed in words, says that a particle coupled to a core with parameters β, γ, λ_F has the same energy spectrum as a hole coupled to a core with parameters β, $60° - \gamma$, $-\lambda_F$. The permutations of the intrinsic axes and the sign change of Δ under transformation Γ have no effect on the energy spectrum.

2.4. The Diagonalization

The Hamiltonian (2.15) is diagonalized in three steps. The first two steps bring $\mathcal{H}_p$ into diagonal form

$$\mathcal{B}^\dagger \mathcal{H}_p \mathcal{B} = \begin{pmatrix} e_\nu & \\ & -e_\nu \end{pmatrix} \tag{2.23}$$

by the unitary transformation

$$\mathcal{B} = \begin{pmatrix} S & \\ & S \end{pmatrix} \begin{pmatrix} U & -V \\ V & U \end{pmatrix} .$$

The unitary transformation S diagonalizes the potential V_p

$$\sum_{\Omega_2}{}' \langle j\Omega_1 | V_p | j\Omega_2 \rangle \, s^{(j)}_{\Omega_2 \nu} = \varepsilon_\nu \, s^{(j)}_{\Omega_1 \nu} , \tag{2.24}$$

yielding the single-particle energies ε_ν. The sum in Eq. (2.24), is restricted to $|\Omega_2| \leqslant j$ and even integers for $(j + \Omega_2)$. The matrices (e_ν), U and V are diagonal; their matrix elements are the quasiparticle energies

$$e_\nu = \sqrt{(\varepsilon_\nu - \lambda_F)^2 + \Delta^2} \tag{2.25}$$

and the BCS-occupation probabilities

$$v_\nu^2 = \frac{1}{2}\left(1 - \frac{\varepsilon_\nu - \lambda_F}{e_\nu}\right) , \tag{2.26a}$$

$$u_\nu^2 = 1 - v_\nu^2 , \tag{2.26b}$$

respectively. The total wavefunction (2.16) is now spanned by new basic states

$$|K\nu\rangle = \sqrt{\frac{2I+1}{16\pi^2}}\left(D^{(I)}_{MK}|\nu\rangle + (-)^{I-j} D^{(I)}_{M-K}|-\nu\rangle\right) \tag{2.27}$$

with

$$|\pm\nu\rangle = \sum_\Omega{}' s^{(j)}_{\Omega\nu} \chi^{(j)}_{\pm\Omega}$$

and the sum restricted to $|\Omega| \leqslant j$ and even integers for $(j+\Omega)$. In this new space, $\mathcal{H}_R$ is obtained as

$$\mathcal{B}^\dagger \mathcal{H}_R \mathcal{B} = \begin{pmatrix} h^{KK'}_{\mu\nu}\ \xi_{\mu\nu} & -h^{KK'}_{\mu\nu}\ \eta_{\mu\nu} \\ h^{KK'}_{\mu\nu}\ \eta_{\mu\nu} & h^{KK'}_{\mu\nu}\ \xi_{\mu\nu} \end{pmatrix} , \tag{2.28}$$

where

$$h^{KK'}_{\mu\nu} = \langle K\mu|h_R|K'\nu\rangle , \tag{2.29}$$

and

$$\xi_{\mu\nu} = u_\mu u_\nu + v_\mu v_\nu , \tag{2.29b}$$

$$\eta_{\mu\nu} = u_\mu v_\nu - v_\mu u_\nu .$$

In the actual calculations, expression (2.28) will be approximated by

$$\mathcal{B}^\dagger \mathcal{H}_R \mathcal{B} \cong \begin{pmatrix} h^{KK'}_{\mu\nu}\ \xi_{\mu\nu} & \\ & h^{KK'}_{\mu\nu}\ \xi_{\mu\nu} \end{pmatrix} , \tag{2.30}$$

so that the final diagonalization of $\mathcal{H} = \mathcal{H}_p + \mathcal{H}_R$ comes down to

$$\sum_{K',\nu}{}' \left(h_{\mu\nu}^{KK'} \xi_{\mu\nu} \pm e_\nu \delta_{KK'} \delta_{\mu\nu} \right) t_{K'\nu,n}^{(I,j)} = E_n^{(I,j)} t_{K\mu,n}^{(I,j)} \qquad (2.31)$$

with the summation restricted to $|K'| \leqslant I$, $(j + K')$ even, and $1 \leqslant \nu \leqslant (j + \frac{1}{2})$. There are $(I + \frac{1}{2}) \cdot (j + \frac{1}{2})$ eigenvalues $E_n^{(I,j)}$ with total angular momentum I for the rotor-plus-particle system and an equivalent set of eigenvalues for the rotor-plus-hole system for which the minus sign in Eq. (2.31) holds. The two sets of eigenvalues are connected by the particle-hole symmetry (2.22) which gives

$$E_n^{(I,j)}(\beta,\gamma,\lambda_F \text{ ; particle}) = E_n^{(I,j)}(\beta,60^\circ - \gamma, -\lambda_F \text{; hole}) . \qquad (2.32)$$

Expression (2.30) which neglects the coupling between quasiparticles and quasiholes holds exactly if the Fermi energy is placed well above or well below the single j-shell, since then $\eta_{\mu\nu} = 0$. But even in the case when the Fermi energy penetrates the energy region of the single-particle states, the approximation $h_{\mu\nu}^{KK'} \eta_{\mu\nu} \simeq 0$ is justified since

$$\eta_{\mu\nu} = 0 \qquad \text{for } \mu = \nu \ , \qquad (2.33a)$$

$$\eta_{\mu\nu} \cong 0 \qquad \text{for } \mu \neq \nu \text{ and } |\varepsilon_\mu - \varepsilon_\nu| < 2\Delta \ ,$$

and, on the other hand,

$$h_{\mu\nu}^{KK'} << \overline{h_{\lambda\lambda}^{KK}} \qquad \text{for } \mu \neq \nu \text{ and } |\varepsilon_\mu - \varepsilon_\nu| > 2\Delta \ , \qquad (2.33b)$$

where $\overline{h_{\lambda\lambda}^{KK}}$ is an averaged diagonal matrix element. The latter estimate

is based on the fact that the Coriolis and centrifugal terms

$$h_{\mu\nu}^{KK'} = \sum_{\kappa=1}^{3} (-2 \langle K\mu \mid I_\kappa j_\kappa \mid K'\nu \rangle + \langle K\mu \mid j_\kappa^2 \mid K'\nu \rangle)/2\mathcal{J}_\kappa$$

predominantly couple neighboring single-particle states and second neighbors which differ less than 2Δ in energy -- at least for weakly deformed nuclei ($0.1 < \beta < 0.2$) which are considered in this work.

2.5. Moments and Transition Probabilities

The quadrupole operator

$$\mathcal{Q}_{2\mu} = \mathcal{Q}_{2\mu}^{(C)} + \mathcal{Q}_{2\mu}^{(p)} \tag{2.34}$$

consists of two parts, one referring to the core

$$\mathcal{Q}_{2\mu}^{(C)} = q_{2\mu}^{(\kappa)} \begin{pmatrix} 1 & & \\ & & \\ & & 1 \end{pmatrix} , \tag{2.35}$$

and the other referring to the odd nucleon

$$\mathcal{Q}_{2\mu}^{(p)} = e^{(p)} \sqrt{\frac{16\pi}{5}}\, r^2\, Y_{2\mu} \begin{pmatrix} 1 & & \\ & & \\ & & -1 \end{pmatrix} , \tag{2.36}$$

where $e^{(p)} = e$ for protons and $e^{(p)} = 0$ for neutrons. The intrinsic quadrupole tensor of the core is given by

$$\begin{aligned} q_{20}^{(\kappa)} &= Q_o \cos\left(\gamma - \frac{2\pi}{3}\kappa\right) , \\ q_{22}^{(\kappa)} &= q_{2-2}^{(\kappa)} = \frac{Q_o}{\sqrt{2}} \sin\left(\gamma - \frac{2\pi}{3}\kappa\right) , \\ q_{21}^{(\kappa)} &= q_{2-1}^{(\kappa)} = 0 , \end{aligned} \tag{2.37}$$

where $\kappa = 1,2,3$ denotes the axis to which the projection μ is related, and

$$Q_o = \frac{3}{\sqrt{5\pi}} R_o^2 Z \beta \tag{2.38}$$

is the intrinsic charge quadrupole moment, R_o the nuclear radius, and Z the charge number. The magnetic dipole operator is defined as

$$\vec{\mathcal{M}} = \left[g_R \vec{I} + \left(g_\ell - g_R \pm \frac{g_\ell - g_s}{2\ell + 1} \right) \vec{j} \right] \begin{pmatrix} 1 & \\ & 1 \end{pmatrix} \tag{2.39}$$

for $j = \ell \pm \frac{1}{2}$, and with $g_R = \frac{Z}{A}$, $g_s = 0.6\, g_s^{free}$, and $g_\ell = 1$ for protons and $g_\ell = 0$ for neutrons.

It can be shown that the operators $\mathcal{Q}$ and $\mathcal{M}$ transform under the particle-hole transformation $(\sigma_y \Gamma)$ as

$$(\sigma_y \Gamma)^\dagger \mathcal{Q}_{2\mu} (\sigma_y \Gamma) = -\mathcal{Q}_{2\mu} \quad , \tag{2.40}$$

$$(\sigma_y \Gamma)^\dagger \vec{\mathcal{M}} (\sigma_y \Gamma) = \vec{\mathcal{M}} \quad . \tag{2.41}$$

These relations represent a generalized particle-hole conjugation in the combined quasiparticle-core system. Equations (2.40) and (2.41) can be proved by using the definitions (2.19) and the symmetry $\Gamma^\dagger q_{2\mu}^{(\kappa)} \Gamma = -q_{2\mu}^{(\kappa)}$ which involves the transformation $\gamma \to 60° - \gamma$ and a cyclic permutation of the intrinsic axes. Due to the symmetries (2.40) and (2.41), all reduced matrix elements of $Q_{2\mu}$ change sign when going from a particle case with parameters β, γ, λ_F to a hole case with parameters β, $60° - \gamma$, $-\lambda_F$, but remain unchanged for the magnetic operator $\vec{M}$.

For particle states, the reduced matrix elements of $Q_{2\mu}^{(C)}$, $Q_{2\mu}^{(p)}$, and

$\vec{M}$ are obtained in the form

$$\langle I',\alpha' \| Q^{(C)} \| I,\alpha \rangle = F^{(C)}_{I'\alpha',I\alpha} \; Q_o \quad , \tag{2.42a}$$

$$\langle I',\alpha' \| Q^{(p)} \| I,\alpha \rangle = F^{(2)}_{I'\alpha',I\alpha} \; q_{s.p.} \quad , \tag{2.42b}$$

and, for $(I',\alpha') \neq (I,\alpha)$,

$$\langle I',\alpha' \| M \| I,\alpha \rangle = F^{(1)}_{I'\alpha',I\alpha} \; (\mu_{s.p.} - g_R j) \quad , \tag{2.42c}$$

where $q_{s.p.}$ and $\mu_{s.p.}$ are the single-particle values for the quadrupole moment and the magnetic moment

$$q_{s.p.} = -\frac{2j-1}{2j+2}\langle r^2 \rangle \quad , \tag{2.43}$$

$$\mu_{s.p.} = \left(g_\ell \pm \frac{g_s - g_\ell}{2\ell+1} \right) j \quad , \tag{2.44}$$

and $\langle r^2 \rangle \cong \left(n + \frac{3}{2}\right) \cdot A^{1/3}[fm^2]$ for the (n,j,ℓ) shell. In Eqs. (2.42), the effect of the rotating core on the matrix elements is contained in the the F-factors which are given by

$$F^{(C)} = \sqrt{(2I'+1)(2I+1)} \sum_{K,K',\Omega,\nu}{}' w^{(I'\alpha',I\alpha,2)}_{K'\Omega,K\Omega} \; (-)^{I'-K'} \begin{pmatrix} I' & 2 & I \\ -K' & \nu & K \end{pmatrix} q_{2\nu}/Q_o \quad , \tag{2.45a}$$

$$F^{(\lambda)} = \sqrt{(2I'+1)(2I+1)} \sum_{K,K',\Omega,\Omega',\nu}{}' w^{(I'\alpha',I\alpha,\lambda)}_{K'\Omega',K\Omega} \; (-)^{I'-K'} \; (-)^{j-\Omega'} \; * \tag{2.45b}$$

$$* \left[\begin{pmatrix} I' & \lambda & I \\ -K' & \nu & K \end{pmatrix} \begin{pmatrix} j & \lambda & j \\ -\Omega' & \nu & \Omega \end{pmatrix} + (-)^{I-j} \begin{pmatrix} I' & \lambda & I \\ -K' & \nu & -K \end{pmatrix} \begin{pmatrix} j & \lambda & j \\ -\Omega' & \nu & -\Omega \end{pmatrix} \right] \Bigg/ \begin{pmatrix} j & \lambda & j \\ -j & 0 & j \end{pmatrix} ,$$

for $\lambda = 1,2$. The summations are restricted as in Eq. (2.16). The amplitude

$$w^{(I'\alpha',I\alpha,\lambda)}_{K'\Omega',K\Omega} = \sum_{\kappa,\kappa'=1}^{(j+\frac{1}{2})} s^{(j)}_{\Omega'\kappa'}\; t^{(I',j)}_{K'\kappa',\alpha'} \left(u_\kappa, u_\kappa - (-)^\lambda v_\kappa, v_\kappa\right) s^{(j)}_{\Omega\kappa}\; t^{(I,j)}_{K\kappa,\alpha} \tag{2.46}$$

includes all the information on the wavefunction. From the reduced matrix elements (2.42), one obtains for the spectroscopic quadrupole moments and the magnetic moments

$$Q^{(sp)}_{I\alpha} = \begin{pmatrix} I & 2 & I \\ -I & 0 & I \end{pmatrix} \langle I\alpha \,\|Q\|\, I\alpha\rangle \quad , \tag{2.47}$$

$$\mu_{I\alpha} = g_R I + \begin{pmatrix} I & 1 & I \\ -I & 0 & I \end{pmatrix} \langle I\alpha \,\|M\|\, I\alpha\rangle \quad , \tag{2.48}$$

and for the reduced E2- and M1-transition probabilities

$$B(E2;\, I\alpha \to I\alpha') = \frac{5}{16\pi} \left|\langle I'\alpha' \,\|Q\|\, I\alpha\rangle\right|^2 / (2I+1) \quad , \tag{2.49}$$

$$B(M1;\, I\alpha \to I'\alpha') = \left|\langle I'\alpha' \|\, M \,|I\alpha\rangle\right|^2 / (2I+1) \quad . \tag{2.50}$$

Mixing ratios are defined as

$$\delta(I\alpha \to I'\alpha') = 0.7\; E_\gamma{}^2 \sqrt{\frac{5}{16\pi}}\; \frac{\langle I'\alpha' \|Q\| I\alpha\rangle}{\langle I'\alpha' \|M\| I\alpha\rangle} \quad , \tag{2.51}$$

where $E_\gamma = (E_I - E_{I'})$ is the transition energy in MeV. The expressions (2.47) - (2.51) correspond to particles coupled to the rotor; the results for holes are obtained by applying the particle-hole transformations (2.40) and (2.41) which reverse the sign of $Q^{(sp)}$ and δ, but leaves all other quantities unchanged.

2.6. The Parameters

The free parameters of the model are β, γ, and λ_F. The general dependence of the energy spectrum and the transition probabilities on these parameters will be discussed in the next chapter. For a particular odd-A nucleus, β and γ will be determined from the lowest excited states of the adjacent even nuclei, and λ_F will be estimated from the Nilsson level scheme. All other parameters are chosen as a smooth function of the mass A, e.g. k and Δ, or as a function of β and A, e.g. $\mathcal{J}_0$.

The strength k of the deformed field of the core is taken as

$$k = \int_0^\infty dr\, r^2 \big(f(r)\big)^2\, k(r) = \frac{206}{A^{1/3}}\ [\mathrm{MeV}] \tag{2.52}$$

consistent with the splitting of the $h_{11/2}$ shell in the Nilsson level scheme. The inertia parameter $\mathcal{J}_0$ is determined by the relation

$$\frac{\hbar^2}{2\mathcal{J}_0} = \frac{204}{\beta^2 \cdot A^{7/3}}\ [\mathrm{MeV}] \tag{2.53}$$

which is derived from the general empirical rule

$$E_{2^+} \cdot B(E2;\, 2^+ \to 0^+) \cong (2.5 \pm 1) \cdot 10^{-3} \cdot Z^2 \cdot A^{-1}\ [\mathrm{MeV} \cdot (\mathrm{eb})^2]\,. \tag{2.54}$$

As shown by Grodzins[10], relation (2.54) holds for first excited 2^+ states almost throughout the nuclear mass table. Both relations (2.52) and (2.53) have been derived assuming axially symmetric deformations. In this work, however, they are considered to hold also for triaxial deformations. The slight γ-dependence of E_{2^+} and $B(E2;\, 2^+ \to 0^+)$ in the Davydov model can be neglected in view of the uncertainty involved in relation (2.54).

The pairing potential is chosen as

$$\Delta = \frac{135}{A} \text{ [MeV]} \tag{2.55}$$

consistent with odd-even mass differences in the mass region $100 < A < 200$. Choosing an A^{-1} dependence for Δ rather than the more general $\Delta \cong 12 \cdot A^{-\frac{1}{2}}$ relation[9]) has the advantage that it preserves a general scale property of the model. Using the inertia parameter (2.53) as energy unit, one obtains from Eqs. (2.52), (2.53), and (2.54)

$$\frac{k\beta}{(\hbar^2/2\mathcal{J}_0)} = 1.01 \cdot (\beta \cdot A^{2/3})^3 \ , \tag{2.56}$$

and

$$\frac{\Delta}{(\hbar^2/2\mathcal{J}_0)} = 0.66 \cdot (\beta \cdot A^{2/3})^2 \ . \tag{2.57}$$

It is seen that the model now contains both β and A only in the combination

$$b = \beta \cdot A^{2/3} \ . \tag{2.58}$$

The energy spectrum of the model obtained for a certain mass A can therefore be applied also to other mass regions using the scale transformations (2.53) and (2.58).

Finally, it should be noticed that the model solution depends only weakly on the angular momentum of the j-shell. The solution for a $j = 11/2$ shell presented in the next chapter therefore is a good approximation for other j-shells, e.g., for the $j = 9/2$ and $j = 13/2$ shell.

3. NUMERICAL RESULTS AND THEIR PHYSICAL INTERPRETATION

In this chapter the energy spectrum, moments, and transition probabilities of the triaxial odd-A system are given as functions of the model parameters β, γ, and λ_F. The equations of the model are solved numerically, and the results are presented in a series of plots providing a survey over that part of the model solution which turns out to be of most interest for actual transitional nuclei. The results are then interpreted in a qualitative way; good analytic approximations have not yet been found.

3.1. Some Properties of the Triaxial Core

Since the features of the odd-A system are closely related to those of the even core, some properties of the core will be discussed briefly at this point and listed for further reference. More details are given, e.g., in the work of Davydov[6]) and in Davidson's book[11]).

The moments-of-inertia $\mathcal{J}_\kappa$ ($\kappa = 1,2,3$) defined by Eq. (2.14) are shown as functions of γ in fig. 1, and the corresponding lowest states of the triaxial even rotor are given in fig. 2. Besides the normal rotational band, a second 2^+ state and other additional states are seen to come down in energy as a function of γ, marking the triaxial region. The energies of the first and second 2^+ state can be expressed analytically[6])

$$E_{2^+_{1,2}} = \frac{6\hbar^2}{2\mathcal{J}_o} \frac{9 \mp \sqrt{81 - 72\sin^2(3\gamma)}}{4\sin^2(3\gamma)} , \qquad (3.1)$$

and the transition probabilities to the groundstate are

$$B(E2; 2^+_{1,2} \to 0^+) = \frac{5}{16\pi} Q_0^2 \cdot \frac{1}{10} \left[1 \pm \frac{3 - 2\sin(3\gamma)}{\sqrt{9 - 8\sin(3\gamma)}} \right] . \qquad (3.2)$$

In Eqs. (3.1) and (3.2), the upper sign refers to the 2^+_1 state and the lower sign to the 2^+_2 state.

A general analytical solution exists for the even triaxial rotor at $\gamma = 30°$. Since this solution provides some insight into the triaxial dynamics and is not found in the literature, it will be given here. Since two moments-of-inertia are equal $\mathcal{J}_2 = \mathcal{J}_3$ at $\gamma = 30°$, as seen in fig. 1, the Hamiltonian (2.12) becomes axially symmetric about the $\hat{1}$-axis for $\gamma = 30°$ (although the shape does not!) and can be written as

$$h_R = a[R_1^2 + 4(R_2^2 + R_3^2)]$$

with $a = 3\hbar^2/8\mathcal{J}_o$. Due to the symmetry, the angular momentum $\vec{R}$ has a sharp projection α on the $\hat{1}$-axis; α has to be an even integer. The energy spectrum is obtained in the form

$$E_{I,\alpha} = a[\alpha^2 + 4(I(I+1) - \alpha^2)] , \qquad (3.3)$$

and the wavefunctions are

$$\Psi_{IM,\alpha} = \sqrt{\frac{2I+1}{16\pi^2(1+\delta_{\alpha,o})}} \left(D^{(I)}_{M\alpha} + (-)^I D^{(I)}_{M-\alpha} \right) . \qquad (3.4)$$

The general expression for the E2-transition probabilities is

$$B(E2; I_1\alpha_1 \to I_2\alpha_2) = \frac{(5/16\pi)(2I_2+1)}{(1+\delta_{\alpha_1,0})(1+\delta_{\alpha_2,0})} \left\{ \begin{pmatrix} I_1 & I_2 & 2 \\ \alpha_1 & -\alpha_2 & 0 \end{pmatrix} q^{(1)}_{20} + (-)^{I_1} \begin{pmatrix} I_1 & I_2 & 2 \\ -\alpha_1 & -\alpha_2 & 0 \end{pmatrix} q^{(1)}_{20} \right.$$

$$\left. + \left[\begin{pmatrix} I_1 & I_2 & 2 \\ \alpha_1 & -\alpha_2 & 2 \end{pmatrix} + \begin{pmatrix} I_1 & I_2 & 2 \\ \alpha_1 & -\alpha_2 & -2 \end{pmatrix} + (-1)^{I_1} \begin{pmatrix} I_1 & I_2 & 2 \\ -\alpha_1 & -\alpha_2 & 2 \end{pmatrix} \right] q^{(1)}_{22} \right\}^2 , \quad (3.5)$$

where, according to Eq. (2.37), the intrinsic quadrupole moments related to the $\hat{1}$-axis are obtained as $q^{(1)}_{20} = 0$ and $q^{(1)}_{22} = \frac{Q_o}{\sqrt{2}}$ for $\gamma = 30°$. The spectroscopic quadrupole moments vanish for all states (I,α) at $\gamma = 30°$

$$Q^{(sp)}_{I\alpha} = 0 \quad , \quad (3.6)$$

since they are proportional to $q^{(1)}_{20}$. It is convenient to introduce the so-called wobbling quantum number[12]) $n = I-\alpha$, since states with same n are connected by large B(E2)-values (3.5). Inserting $\alpha = I-n$, Eq. (3.3) reads

$$E_{I,n} = a[I(I+4) + 3n(2I-n)] \quad , \quad (3.3a)$$

where $(I-n)$ has to be an even integer > 0. The quantum number n labels a series of rotational bands with $I = n, n+2, n+4, \ldots$ $(n > 0)$ parallel to the Yrast band with $I = 0,2,4, \ldots$ $(n = 0)$. In connection with the low-excited odd-A spectrum, one is interested in the lowest states of the core spectrum, in particular, in the first and second 2^+ state. For these two states, the precession of $\vec{R}$ about the $\hat{1}$-axis is illustrated in fig. 3. For the 2^+_1 state $(n = 0)$ $\vec{R}$ shows maximal alignment with the $\hat{1}$-axis, whereas for the 2^+_2 state $(n = 2)$ $\vec{R}$ has a zero projection on the $\hat{1}$-axis and is confined to the $(\hat{2}, \hat{3})$ plane. The usual characterization of the 2^+_2

state as a γ-bandhead having a $K = 2$ projection on the $\hat{3}$-axis holds only approximately in the region $0° < \gamma < 15°$.

3.2. The Odd-A Energy Spectrum

The odd-A energy spectrum is obtained as a numerical solution of Eq. (2.31). The single-particle energies ε_ν ($\nu = 1,2, \ldots j+\frac{1}{2}$) which enter that calculation are given as functions of γ in fig. 4. They represent the splitting of the pure $j = 11/2$ shell in the field of the triaxial core. Going from the prolate to the oblate side at a fixed β by changing γ from 0° to 60°, the single-particle energies change smoothly without crossing each other. The single-particle wavefunctions have a sharp Ω quantum number at $\gamma = 0°$ and $\gamma = 60°$, but represent a mixture of different Ω-states in the triaxial region. The thin lines in fig. 4 show the energies ε_ν as they change with β at $\gamma = 0°$ corresponding to a Nilsson level scheme.

The energy spectrum of the odd nucleon coupled to the rotating core is shown in figs. 5 - 7 for different sets of the parameters β, γ, and λ_F. These sets have been chosen to cover that part of the parameter space $4 < \beta \cdot A^{2/3} < 7$, $0° < \gamma < 60°$, $\lambda_F < \varepsilon_2$ which is of most interest for actual transitional nuclei in the $A = 135$ and the $A = 190$ mass region. The plots 5 - 7 apply to particle spectra; due to the particle-hole symmetry (2.22) the corresponding hole spectra are obtained by changing γ, λ_F into $(60° - \gamma)$, $-\lambda_F$.

In figs. 5a, 5b, 5c the odd-A spectrum is shown as a function of β, in fig. 5a for axially symmetric deformations and $\lambda_F = \varepsilon_1$, in fig. 5b and 5c for $\gamma = 30°$ with $\lambda_F = \varepsilon_1$ and $\lambda_F = \varepsilon_2$, respectively. In the weak coupling

region $|\beta \cdot A^{2/3}| < 4$, the wavefunctions contain rather pure core states, and the spectrum consists of almost degenerate core excitation multiplets. Beyond this region, structures develop which differ appreciably from weak coupling. For axially symmetric deformations, these structures have been discussed by Stephens[1]), and fig. 5a is included here as a starting point. On the oblate side ($\beta < 0$) a strongly-coupled rotational band with spin sequence j, j+1, j+2 ... is seen, whereas on the prolate side ($\beta > 0$) a decoupled rotational band appears with spin sequence j, j+2, j+4 ... and energy spacings which are approximately those of the core; for large $\beta \cdot A^{2/3}$, an $\Omega = \frac{1}{2}$ band with a decoupling factor a = 6 is seen to develop. It is important to note that all other levels rise steeply in energy with increasing deformation and leave the energy region below 30 $\hbar^2/2\mathcal{J}_0$ with relatively small level density. The larger level density observed in experimental cases will be one indication for the presence of triaxial shapes.

The spectrum at $\gamma = 30°$, shown in fig. 5b and 5c, differs from fig. 5a mainly due to additional low-excited states emerging from the second 2_2^+ state of the core. These levels behave differently from those of the first 2_1^+ state. As seen in fig. 5b, the 9/2 and the 11/2 levels stemming from the 2_1^+ state rise more steeply with increasing β and exchange at a deformation $\beta \cdot A^{2/3} \simeq 5$ with the corresponding levels coming from the 2_2^+ state. This level exchange leads to pronounced variations in the decay properties of the first and second excited j and (j - 1) levels and therefore provides another test for the present model.

In fig. 5c the Fermi energy $\lambda_F = \varepsilon_2$ has been placed on the second

single-particle level which has a good $\Omega = 9/2$ for $\gamma = 60°$ as seen in fig. 4. The penetration of λ_F into the system of single-particle energies which is equivalent to filling the j-shell mainly causes a lowering of the $(j - 1 = 9/2)$ state and states depending thereon with spins $j+1$, $j+3$, ... The dropping of the $(j-1)$ state when filling a j-shell is observed throughout the nuclear table, and the quasiparticle description applied in this work is a simple means to account for this behavior.

In figs. 6a and 6b, the dependence of the spectrum on γ is shown, in fig. 6a for $\beta \cdot A^{2/3} = 7$ and $\lambda_F = \varepsilon_2$. It is observed that the odd-A spectrum is not symmetric about $\gamma = 30°$ as the core spectrum, shown in fig. 2, but that it changes in a characteristic way from the decoupled structure at $\gamma = 0°$ to the strongly-coupled structure at $\gamma = 60°$. The spectrum at $\gamma = 60°$ consists of an $\Omega = 11/2$ groundband and $\Omega = 9/2$ and $\Omega = 7/2$ excited bands. It is the variety of intermediate situations as γ changes which gives each γ-region a definite signature and opens a wide field for testing the model in actual nuclei. For example, the favored Yrast states having spins j, $(j+2)$, ... are crossing with those having spins $(j+1)$, $(j+3)$, ... in the region $20° < \gamma < 30°$; the group of low-spin states $(I < j)$ moves in a specific way against the group of high-spin states $(I > j)$ with the $(j-2)$-state, e.g., crossing the $(j+1)$ and the $(j+2)$-state in the region $30° < \gamma < 40°$; second and third states of each spin are seen to come down in energy in the region $20° < \gamma < 40°$ (parallel to the corresponding states of the core seen in fig. 2) producing a number of near-crossings of states with the same spin, each marking a certain γ. The positions of these near-crossings, however, also depend

strongly on β and λ_F. Placing the Fermi energy at $\lambda_F = \varepsilon_2$, as done in fig. 6b, the lower part of the spectrum merges into an $\Omega = 9/2$ groundband at $\gamma = 60°$ rather than an $\Omega = 11/2$ band; the $\Omega = 11/2$ band now appears as an excited band.

The dependence of the odd-A spectrum on λ_F, with λ_F passing the whole range of the single-particle energies, is shown in fig. 7 for $\gamma = 30°$ and $A^{2/3} = 7$. It should be noticed that the spectrum does not depend on λ_F as long as λ_F lies outside the j-shell. Penetrating the j-shell has the strongest effect on the low-spin states with $I = (j-1)$, $(j-3)$ and on the $(j-2)$ and $(j-4)$ state when λ_F approaches ε_3. The symmetry in fig. 7 about $\lambda_F = 0$ is a consequence of the particle-hole symmetry (2.22) which gives $E(\beta, \gamma = 30°, \lambda_F) = E(\beta, 60° - \gamma = 30°, -\lambda_F)$.

3.3. Calculated Moments and Transition Probabilities

Some moments and transition probabilities, calculated according to the equations of section 2.5., are given as functions of γ in figs. 8 - 10 for $\beta \cdot A^{2/3} = 5$ and $\lambda = \varepsilon_1$. All plots refer to odd-neutron nuclei. The spectroscopic quadrupole moments Q^{sp} and the E2-transition probabilities therefore contain only contributions of the core. Since the single-particle contribution in the case of odd protons adds less than 10%, plot 8 and 9 apply approximately to odd-proton nuclei also. In the case of nucleon-holes coupled to the rotor one has to change $\gamma \to (60° - \gamma)$, $\lambda_F \to -\lambda_F$, $Q^{sp} \to -Q^{sp}$, $\delta \to -\delta$; the B(E2) values remain unchanged.

The Q^{sp} of the odd-A nucleus, shown in fig. 8 for some of the lowest states, are all negative in the whole region $0° \leqslant \gamma \leqslant 60°$. This is in contrast to the Q^{sp} of even triaxial nuclei, where e.g. the $Q^{sp}_{2_1^+}$

change from $-2/7\ Q_o$ at $\gamma = 0°$ to $+2/7\ Q_o$ at $\gamma = 60°$ and vanish for $\gamma = 30°$ as stated by Eq. (3.6). The difference in the behavior is caused by the odd particle which, as a general rule, tends to adjust itself to the core in such a way that the core adds to the single-particle quadrupole moment with the same sign. It will be discussed in the next section that this adjustment corresponds to a minimum of the potential energy.

The E2-transition probabilities given in fig. 9 vary strongly as functions of γ and therefore provide another possibility for testing the model. The change from strongly collective values to small values of single-particle strength is especially pronounced for the $(j+2) \to j$, $(j+1) \to j$, and $(j-2) \to j$ transitions. For the $(j+2) \to (j+1)$ and the $(j-1) \to (j-2)$ transition, the B(E2)-values vanish at certain γ's; these γ-points are the same at which crossings of the corresponding energies occur and where the signs of the mixing ratios $\delta(I_1 \to I_2)$ change, as seen in fig. 10. Instead of the mixing ratios (2.51), fig. 10 gives the ratios

$$\delta' = \frac{\langle I_2 \| \sqrt{5/16\pi}\, Q \| I_1 \rangle}{\langle I_2 \| M \| I_1 \rangle} ,$$

which are independent of the transition energy. They have a dimension and are given in units $Q_o/(\mu_{s.p.} - g_R j)$. The quantities Q_o and $\mu_{s.p.}$ are defined in Eqs. (2.38) and (2.44), and $g_R = Z/A$.

The signs of δ follow a simple rule expressed in Table 2. This rule has been deduced from the numerical results and holds for all sizable transitions within the low-excited level system. The rule is independent of γ and is found valid at least for $3 < \beta \cdot A^{2/3}$ and $\lambda_F \leqslant \varepsilon_2$.

It was confirmed on the basis of some limiting approximate solutions; a more general justification has still to be given.

The magnetic moments of the lowest states are rather well described by the expression $\mu \cong g_R(I - j) + \mu_{s.p.}$ and do not show any marked dependence on the model parameters. With the choice $g_s = 0.6\, g_s^{free}$, measured magnetic moments are usually well reproduced. M1-transition probabilities can be derived from fig. 9 and fig. 10 using the relation $B(M1;\ I\alpha \to I'\alpha') = \delta'^2 \cdot B(E2;\ I\alpha \to I'\alpha')$.

3.4. The Physical Interpretation

The dynamics of the coupled system of the odd nucleon and the rotating core are based on three physical mechanisms:

(i) The dynamics of the triaxial core which are determined by the three moments-of-inertia and which prefer rotation about the axis with the largest moment-of-inertia in order to minimize the rotational energy.

(ii) The coupling of the odd nucleon to the core which prefers maximal mass overlap (since the nucleon in the high-j shell has an oblate density distribution which is axially symmetric about the direction of its angular momentum $\vec{j}$, strongest coupling occurs with an oblate core at $\gamma = 60°$).

(iii) The interaction between the angular momenta of the odd nucleon $\vec{j}$ and the rotating core $\vec{R}$ due to centrifugal and Coriolis forces; the corresponding energy is minimal for parallel alignment of $\vec{j}$ and $\vec{R}$.

If alignment of $\vec{j}$ and $\vec{R}$ can be achieved, the odd nucleon does not contribute appreciably to the rotational energy of the system, and the lowest rotational band is essentially that of the core, but with a spin sequence $j, j+2, j+4 \ldots$. These bands are called decoupled. If, however, mechanisms (i) and (ii) force $\vec{j}$ and $\vec{R}$ to stand perpendicular on each other, strongly-coupled rotational bands with spin sequence $j, j+1, j+2, \ldots$ show up.

The moments-of-inertia and the way they depend on γ play a decisive role in the question which of the two situations occur. Since, due to mechanism (ii), $\vec{j}$ tends to align with the $\hat{2}$-axis which becomes the oblate symmetry axis at $\gamma = 60°$, the question is in particular how the moment-of-inertia $\mathcal{J}_2$ changes with γ. For the moments-of-inertia (2.14) used in this work, $\mathcal{J}_2 \to 0$ when $\gamma \to 60°$, as shown in fig. 1. This means that, as γ approaches the oblate shape, rotation about the $\hat{2}$-axis becomes increasingly unfavorable and that $\vec{R}$ is pushed into the $(\hat{1}, \hat{3})$-plane perpendicular to $\vec{j}$. As a result, strongly-coupled bands build up in the oblate region as seen in fig. 6.

The moment-of-inertia about the symmetry axis of an axially symmetric core vanishes for symmetry reasons, but no such argument exists in the triaxial region. The actual moments-of-inertia could differ from the values (2.14). If one would use, e.g., moments-of-inertia

$$\mathcal{J}_\kappa^{\text{rig}} = \mathcal{J}_0\left(1 + \sqrt{\frac{5}{4\pi}}\,\beta\cos\left(\gamma - \frac{2\pi}{3}\kappa\right)\right) \quad , \quad \kappa = 1,2,3 \quad ,$$

which depend on γ in the same way as those of a rigid body, the odd-A

spectrum would look quite different, as illustrated in fig. 11. Since then $\mathcal{J}_2^{rig} \neq 0$ for all γ, the decoupled level order would persist in the whole range $0° < \gamma < 60°$. This clearly demonstrates that the characteristic variation of the odd-A energy spectrum as given in fig. 6 and the variety of level crossings decisively depend on the moments-of-inertia (2.14) chosen to be of irrotational type. The comparison of the model with experiment will therefore provide a test not only for triaxial shapes, but to the same extent a test of the moments-of-inertia.

The physics involved in the model are studied in fig. 12 for the first $(j-2)$ state in some more detail. The $(j-2)$ state is distinguished as the lowest excited level in a wide region $0° \leqslant \gamma \leqslant 35°$, as seen in fig. 6. Its energy increases smoothly with γ suggesting that a rather stable coupling structure is underlying. The steady rise in energy breaks off only at about $\gamma = 45°$ due to an interchange of structure with the $\Omega = (j-2)$ Nilsson state. For a prolate core at $\gamma = 0°$, the $(j-2)$ state is described in the rotation-aligned coupling scheme[1]) by an antiparallel alignment of $\vec{j}$ and $\vec{R}$ as shown in the upper part of fig. 12; the corresponding vector system is free to precess in the $(\hat{1}, \hat{2})$-plane about the $\hat{3}$-axis which is the axial symmetry axis at $\gamma = 0°$. However, as γ changes from 0° towards 60°, the rotation-aligned vector system gradually localizes about the $\hat{2}$-axis, since this position is now favored by the potential energy due to mechanism (ii). The coupling to the $\hat{2}$-axis is illustrated for $\gamma = 30°$ in the lower part of fig. 12. It should be noticed that the vector diagram is now approximately equivalent to that of a $\overline{K} = (\overline{\Omega} - 2)$ γ-bandhead.

The gradual localization of the aligned angular momenta about the $\hat{2}$-axis occurs in the same way for other favored Yrast states with $j \pm 2$ $j \pm 4$, ... and gives them the characteristic of $\overline{K} = \overline{\Omega} \pm 2$, $\overline{K} = \overline{\Omega} \pm 4$, ... γ-bandheads. At this point, $\overline{K}$ and $\overline{\Omega}$ are considered as averaged projections of $\vec{I}$ and $\vec{j}$ on the $\hat{2}$-axis; they are *not* good quantum numbers, however can be used for an *approximate* classification. It turns out that Stephens' rotation-aligned coupling scheme, which holds for $\gamma = 0°$, persists when moving into the triaxial region, but, in addition to the alignment of $\vec{j}$ and $\vec{R}$, both now align with the $\hat{2}$-axis. This has an important consequence which distinguishes the triaxial region and can be tested experimentally. On the basis of the additional coupling to the intrinsic $\hat{2}$-axis, one now expects rotational bands with normal spin order to build up on each of the favored Yrast states. The onset of this band structure is indeed present in the model solution as well as in experimental spectra. It will be discussed in the next section.

From the coupling picture derived above, one might approximately consider the excitation energy of the $(j-2)$ state as pure rotational energy about the $\hat{2}$-axis ($\mathcal{J}_2$ taken from Eq. (2.14)):

$$E_{(j-2)} - E_j \cong \frac{(K-\Omega=2)^2}{2\mathcal{J}_2} = \frac{3}{2\sin^2(\gamma - 60°)} \,. \qquad (3.7)$$

In the same kind of classical approximation, one obtains

$$B(E2;\,(j-2) \to j) \cong \frac{5}{16\pi} \left| q^{(2)}_{22} \right|^2 = \frac{5}{16\pi} Q_0^2 \frac{\sin^2(\gamma - 60°)}{2} \,, \qquad (3.8)$$

using expression (2.37) for the quadrupole moment $q_{22}^{(2)}$. As shown in fig. 12, these approximate expressions reproduce the γ-dependence of the exact excitation energy and $B(E2; (j-2) \to j)$ in the right way and confirm that rotation about the $\hat{2}$-axis is indeed the basic mode underlying the $(j-2)$ state in the triaxial region. Due to the coupling to the $\hat{2}$-axis, the $B(E2; (j-2) \to j)$ is quite large even at $\gamma = 30°$ where the 2_2^+ (γ-bandhead) $\to 0^+$ (groundstate) transition of the core is forbidden as seen from Eq. (3.2).

3.5. Classification of States and Band Structures

In the preceding chapters, individual states and their dependence on the model parameters have been studied. The question remains how the states can be classified in a systematic way. A related question is to which extent band structures known from strongly deformed nuclei persist in the transitional region.

The weak coupling classification in terms of core excited states can be used for deformations $|\beta \cdot A^{2/3}| < 4$, but is inadequate in the region $\beta \cdot A^{2/3} > 4$, where the energy spread of the core multiplets becomes larger than the core energy spacings (see fig. 5). Most transitional nuclei around $A = 135$ and $A = 190$ have deformations $4 < \beta \cdot A^{2/3} < 7$. This indicates that the strong coupling classification in terms of projections of $\vec{j}$ and $\vec{I}$ on an intrinsic axis might be more adequate for these nuclei.

As discussed in section 3.4., the odd particle tends to couple to the $\hat{2}$-axis of the triaxial core, and, consequently, this axis will serve

as an approximate symmetry axis. The approximate quantum numbers $\overline{K}$ and $\overline{\Omega}$ are defined in fig. 13. Although the model wavefunctions

$$\psi_{IM,\alpha} = \sum_{K,\Omega} C_{K\Omega}^{(I,j,\alpha)} \left(D_{MK}^{(I)} \chi_{\Omega}^{(j)} + (-1)^{I-j} D_{M-K}^{(I)} \chi_{-\Omega}^{(j)} \right)$$

consist of a mixture of all possible K and Ω components, it is found that most of the lowest energy states have one dominant component $C_{\overline{K}\overline{\Omega}}^{(I,j,\alpha)}$ which determines their approximate $(\overline{K},\overline{\Omega})$ classification. This is demonstrated in Table 3 for the lowest states at $\gamma = 30°$ and $\beta \cdot A^{2/3} = 5$, $\lambda_F = \varepsilon_1$ (see fig. 6a). The $(\overline{K},\overline{\Omega})$ classification of these states is also shown in fig. 14. Some important points should be emphasized:

1. As seen from Table 3, only the very lowest states have dominant (K,Ω) components which represent more than 50% of the wavefunction. It is therefore in a very tentative sense that the $(11/2)_1$, $(13/2)_1$, $(15/2)_2$, $(17/2)_2$ states, given in the first part of the Table, are considered as forming an approximate $\overline{K} = \overline{\Omega} = 11/2$ band. This is even more so for the $(\overline{K} = 15/2,\ \overline{\Omega} = 11/2)$ and the $(\overline{K} = 7/2,\ \overline{\Omega} = 11/2)$ band classification, which relates these states to odd-A γ-bands, and for the higher states classified as $\overline{\Omega} = 9/2$ states. Nevertheless, this classification will turn out to be useful in the analysis of experimental spectra.

2. Although the $(\overline{K},\overline{\Omega})$ classification is weakly defined by the wavefunctions, another strong coupling feature stating that largest B(E2;↓)- and B(M1;↓)-values occur between states *within* a band is found to be rather well developed in the model solution. This is demonstrated

in fig. 14. It shows that there is a strong coupling pattern underlying the calculated odd-A spectrum even for $\beta \cdot A^{2/3} = 5$ and $\gamma = 30°$.

3. However, the coupling is not strong enough to insure that the main decay channels run within the separate bands. Model states lying higher in energy, e.g. those with the $\overline{\Omega} = 9/2$ classification, but also higher states of the $\overline{K} = 11/2$ and $\overline{K} = 7/2$ bands, decay favorably into lower neighboring bands. The comparison with experimental cases in Part II of this work will give evidence for this band leaking.

4. The spectrum at $\gamma = 60°$ and $\beta \cdot A^{2/3} = 5$ is also shown in fig. 14 for comparison. Its low-energy part consists of a rather pure $\overline{K} = \overline{\Omega} = 11/2$ and a $\overline{K} = \overline{\Omega} = 9/2$ band. When going into the triaxial region starting from $\gamma = 60°$, the 11/2- and 9/2-band mix with each other and with other higher bands, thus gradually losing their $(\overline{K},\overline{\Omega})$ character. But it will be noticed that remainders of these bands, at least the lowest members of the 11/2-band, can be identified all over the triaxial region.

5. As a new feature, additional bands with γ-band character $\overline{K} = \overline{\Omega} \pm 2$, $\overline{\Omega} \pm 4$, ... come down in energy in the triaxial region and take over as lowest excited states for $\gamma < 30°$. For γ approaching 0°, the bandheads of these additional bands form the decoupled yrast band.

4. CONCLUSION

The model of an odd nucleon coupled to a rotating triaxial core has been investigated with the aim of providing a basis for a systematic study of transitional odd-A nuclei. Concerning the coupling of the odd nucleon to the core, the model covers the weak-coupling region ($0 < \beta \cdot A^{2/3} < 4$) as well as the strong-coupling region ($\beta \cdot A^{2/3} > 7$) and describes the various intermediate regions as a function of the deformation parameter $\beta \cdot A^{2/3}$ and the asymmetry parameter γ. The γ-degree of freedom is found to play a decisive role in the particle-core coupling. It is observed that the calculated energies, moments, and transition probabilities of the coupled core-particle system are subject to drastic variations when γ changes in the range $0° \leqslant \gamma \leqslant 60°$. This opens a wide field for testing the model experimentally.

A systematic comparison with unique-parity spectra of nuclei in the $A = 190$ and $A = 135$ mass region is given in Part II of this work. The comparison provides strong evidence that the present model indeed applies to transitional odd-A nuclei and that triaxial shapes are a general feature of these nuclei. It turns out that the assumption of rigid triaxial shapes is a better approximation with respect to the particle-core coupling than with respect to the collective motion of the core. Odd-A transitional nuclei therefore represent the real domain of the Davydov approximation. The general solution, given in this paper, may serve as a guide for analyzing odd-A data and may stimulate new experimental work to verify -- or refute -- the numerous trends for energies and transition probabilities predicted by the present work.

ACKNOWLEDGMENTS

The author is indebted to Dr. R. M. Diamond and Dr. F. S. Stephens who proposed this work and followed its progress with continuous interest. In particular, he acknowledges some very helpful discussions concerning the physical interpretation of the numerical results. The author thanks Dr. N. Glendenning for the hospitality of the nuclear theory group.

REFERENCES

[1] F. S. Stephens, Proceedings of the International Conference on Nuclear Physics, Munich, 1973, Editors J. de Boer and H. J. Mang, Vol. II, (North-Holland, Amsterdam, 1973), p. 367 ff., and Rev. Mod. Phys., to be published.

[2] J. Meyer-ter-Vehn, F. S. Stephens, and R. M. Diamond, Phys. Rev. Letters 32 (1974) 1383.

[3] A. Bohr, K. Danske Vidensk. Selsk. mat.-fys. Medd. 26, No. 14 (1952); A. Bohr and B. R. Mottelson, K. Dansk Vidensk. Selsk. mat.-fys. Medd. 27, No. 16 (1953).

[4] K. Kumar and M. Baranger, Nucl. Phys. A92 (1967) 608; K. Kumar and M. Baranger, Nucl. Phys. A122 (1968) 273.

[5] G. Gneuss and W. Greiner, Nucl. Phys. A171 (1971) 449.

[6] A. S. Davydov and G. F. Filippov, Nucl. Phys. 8 (1958) 237; A. S. Davydov and V. S. Rostovsky, Nucl. Phys. 12 (1959) 58.

[7] K. Hecht and G. R. Satchler, Nucl. Phys. 32 (1962) 286; L. W. Pearson and J. O. Rasmussen, Nucl. Phys. 36 (1962) 666.

[8] V. V. Pashkevich, R. A. Sardaryan, Nucl. Phys. 65 (1965) 401; V. V. Pashkevich, Izv. AN SSSR (ser.fiz.) 25 (1961) 782.

[9] A. Bohr and B. R. Mottelson, Nuclear Structure, Vol. I (W. A. Benjamin, New York, 1969).

[10] L. Grodzins, Phys. Letters 2 (1962) 88.

[11] J. P. Davidson, Collective Models of the Nucleus (Academic Press, New York, 1968).

[12] B. R. Mottelson, Proceedings of the Nuclear Structure Symposium of the Thousand Lakes, Joutsa, Finland (1970), p. 148 ff., Univ. Jyväskylä, Research Report No. 4/1971.

Table 1. Values of γ and corresponding symmetry axes for axially symmetric prolate and oblate shapes.

γ	symmetry axis	shape
0°	$\hat{3}$	prolate
60°	$\hat{2}$	oblate
120°	$\hat{1}$	prolate
180°	$\hat{3}$	oblate
240°	$\hat{2}$	prolate
300°	$\hat{1}$	oblate

* * * * * *

Table 2. Sign rule for mixing ratios $\delta(I_1 \rightarrow I_2)$ in odd-A nuclei with the odd nucleon representing either a neutron or a proton and either a particle or a hole.

$\delta(I_1 \rightarrow I_2)$	Neutron		Proton	
$E_{I_1} > E_{I_2}$	particle	hole	particle	hole
$I_1 > I_2$	+	-	-	+
$I_1 < I_2$	-	+	+	-

Table 3. Dominant components $|C^{(I,\, j=11/2)}_{K,\Omega}|^2$ of the wavefunctions for $\gamma = 30°$, $\beta \cdot A^{2/3} = 5$, and $\lambda_F = \varepsilon_1$.

Band	Spin	Energy	$\lvert C_{K,\Omega}\rvert^2$		
11/2	I	$E_I/(\hbar^2/2\mathcal{J}_o)$	$K = \Omega = 11/2$	$K = \Omega = 9/2$	$K = 13/2, \Omega = 9/2$
$\overline{K} = 11/2$	11/2	0.0	0.74	0.14	--
$\overline{\Omega} = 11/2$	13/2	13.0	0.61	0.21	0.01
	15/2	26.8	0.22	0.16	0.05
	17/2	46.8	0.20	0.09	0.16
15/2			$K = 15/2, \Omega = 11/2$	$K = 13/2, \Omega = 9/2$	$K = \Omega = 11/2$
$\overline{K} = 15/2$	15/2	12.0	0.62	0.14	0.09
$\overline{\Omega} = 11/2$	17/2	26.9	0.43	0.14	0.14
	19/2	34.8	0.19	0.11	0.08
	21/2	52.1	0.22	0.14	0.10
7/2			$K = 7/2, \Omega = 11/2$	$K = 5/2, \Omega = 9/2$	$K = \Omega = 9/2$
$\overline{K} = 7/2$	7/2	9.6	0.75	0.12	--
$\overline{\Omega} = 11/2$	9/2	18.1	0.44	0.11	0.33
	11/2	28.3	0.43	0.16	0.22
	13/2	40.4	0.31	0.16	0.13

continued. . .

Table 3 (continued)

Band	Spin	Energy	$\lvert C_{K,\Omega}\rvert^2$		
9/2			$K = \Omega = 9/2$	$K = \Omega = 7/2$	$K = \Omega = 11/2$
$\overline{K} = 9/2$	9/2	20.9	0.32	0.18	--
$\overline{\Omega} = 9/2$	11/2	25.8	0.09	0.14	0.13
	13/2	46.5	0.10	0.10	0.18
13/2			$K = 13/2, \Omega = 9/2$	$K = 11/2, \Omega = 7/2$	$K = 9/2, \Omega = 5/2$
$\overline{K} = 13/2$	13/2	31.2	0.55	0.16	0.06
$\overline{\Omega} = 9/2$	15/2	38.7	0.19	0.10	0.06
5/2			$K = 5/2, \Omega = 9/2$	$K = 3/2, \Omega = 7/2$	$K = \Omega = 5/2$
$\overline{K} = 5/2$	5/2	30.0	0.66	--	0.14
$\overline{\Omega} = 9/2$	7/2	31.6	0.20	0.17	0.04
	9/2	42.3	0.20	0.17	0.06

FIGURE CAPTIONS

Fig. 1. Irrotational moments-of-inertia as functions of γ.

Fig. 2. Low-energy spectrum of an even triaxial core as a function of γ.

Fig. 3. Precession of the angular momentum $\vec{R}$ about the $\hat{1}$-axis of the triaxial core at $\gamma = 30°$ for the first and the second 2^+ state.

Fig. 4. Single-particle energies of a $j = 11/2$ shell in the field of a triaxial core. The heavy lines show the variation with γ, the thin lines the variation with β at $\gamma = 0°$. The numbers on the right and left side give the Ω quantum number of each state for axially symmetric prolate and oblate shapes, respectively.

Fig. 5a. The odd-A energy spectrum as a function of β for $\gamma = 0°$, $\lambda_F = \varepsilon_1$, and $j = 11/2$. The core states underlying the multiplets at $\beta = 0$ are indicated.

Fig. 5b. Same as fig. 5a, but for $\gamma = 30°$ and $\lambda_F = \varepsilon_1$.

Fig. 5c. Same as fig. 5a, but for $\gamma = 30°$ and $\lambda_F = \varepsilon_2$.

Fig. 6a. The odd-A energy spectrum as a function of γ for $\beta \cdot A^{2/3} = 5$, $\lambda_F = \varepsilon_1$, and $j = 11/2$.

Fig. 6b. Same as fig. 6a, but for $\beta \cdot A^{2/3} = 7$ and $\lambda_F = \varepsilon_2$.

Fig. 7. The odd-A energy spectrum as a function of λ_F for $\beta \cdot A^{2/3} = 7$, $\gamma = 30°$, and $j = 11/2$.

Fig. 8. Spectroscopic quadrupole moments of the lowest odd-A states, including the second j state, as functions of γ for $\beta \cdot A^{2/3} = 5$, $\lambda_F = \varepsilon_1$, and $j = 11/2$.

Fig. 9. Reduced E2-transition probabilities for the lowest odd-A states as functions of γ for $\beta \cdot A^{2/3} = 5$, $\lambda_F = \varepsilon_1$, and $j = 11/2$.

Fig. 10. Ratios $\delta' = \langle I_2 \| \sqrt{5/16\pi}\, Q \| I_1 \rangle / \langle I_2 \| M \| I_1 \rangle$ for the lowest odd-A states, including the second j state, as functions of γ for $\beta \cdot A^{2/3} = 5$, $\lambda_F = \varepsilon_1$, and $j = 11/2$. The magnetic unit $\mu_o = \mu_{s.p.} - g_R j$ with $\mu_{s.p.}$ being the single-particle magnetic moment.

Fig. 11. Some lowest energy states of the odd-A spectrum as functions of γ assuming rigid moments-of-inertia with $\beta = 0.3$.

Fig. 12. Schematic illustration of the lowest $(j - 2)$ state. Vector diagrams of $\vec{j}$, $\vec{R}$, $\vec{I}$ and their position relative to the intrinsic axes of the core (shaded area) are shown for $\gamma = 0°$ and $\gamma = 30°$; the dark disk indicates the mass distribution of the odd nucleon. In the central part, the exactly calculated $E_{(j-2)}$ and $B(E2;(j-2) \to j)$ are compared with approximate expressions (broken lines) for $j = 11/2$.

Fig. 13. Vector diagram defining the approximate quantum numbers $\bar{K}$ and $\bar{\Omega}$.

Fig. 14. The $(\bar{K},\bar{\Omega})$ classification of the lowest odd-A states with $\beta \cdot A^{2/3} = 5$, $\lambda_F = \varepsilon_1$, and $j = 11/2$ for $\gamma = 30°$ and $\gamma = 60°$. Solid and broken lines mark transitions with the largest $B(E2;\downarrow)$ and the largest $B(M1;\downarrow)$ for a given level, respectively.

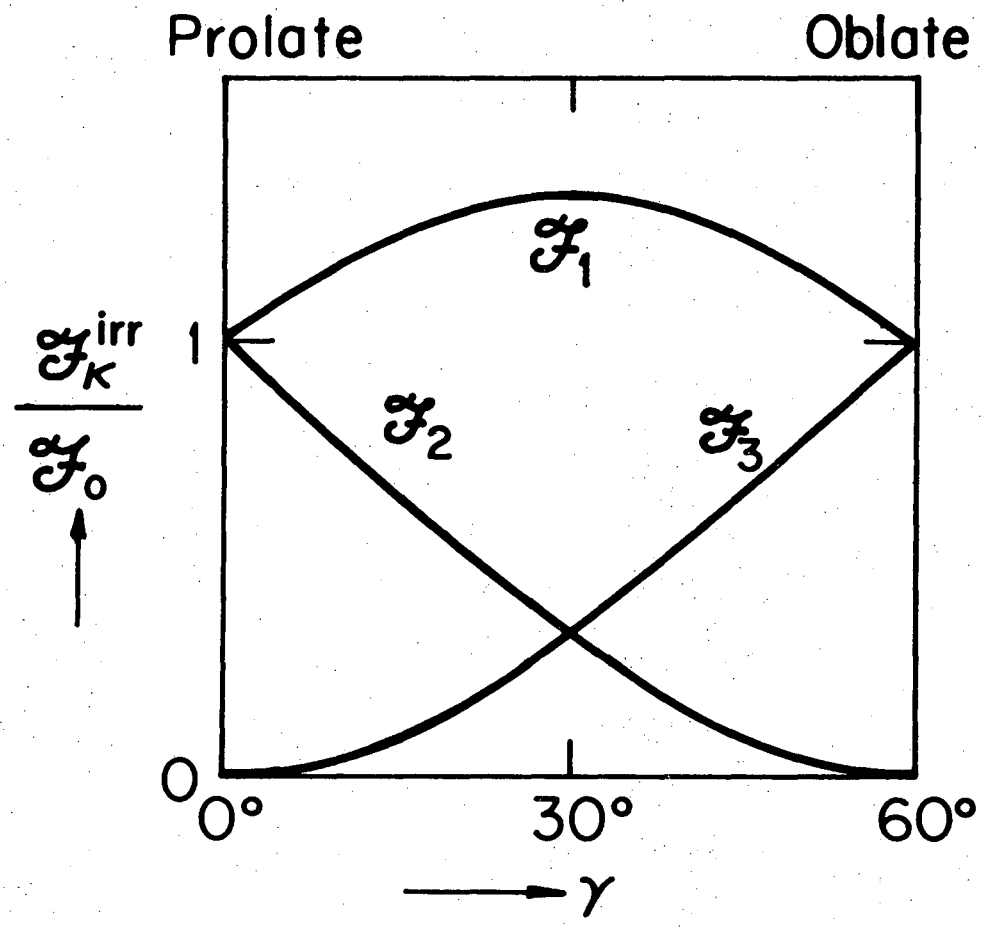
Prolate
Oblate
$\mathcal{F}_K^{irr}$
$\mathcal{F}_0$
1
0
$\mathcal{F}_1$
$\mathcal{F}_2$
$\mathcal{F}_3$
0°
30°
60°
γ
XBL7410-4394

Fig. 1

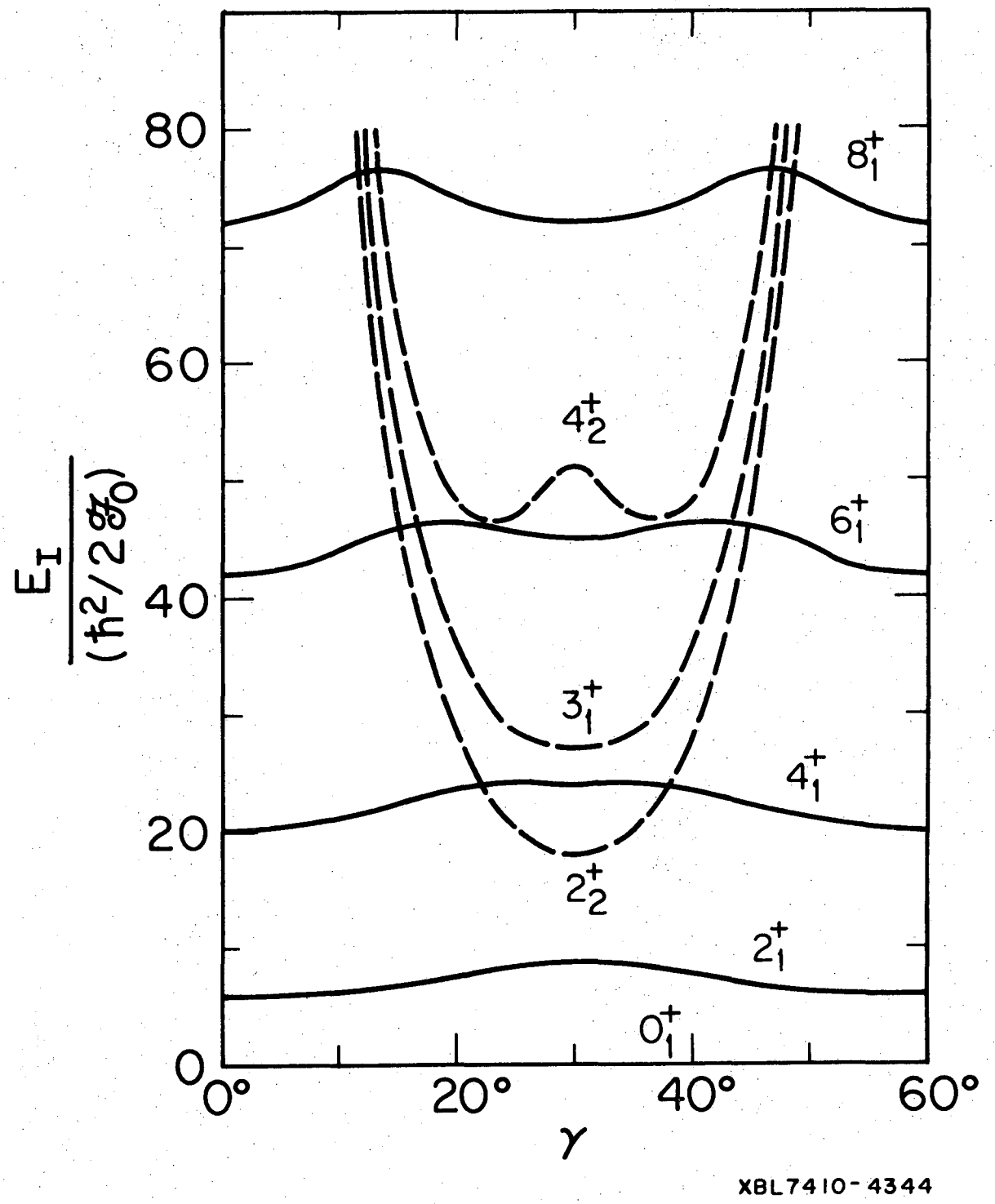
80
60
40
20
0
0°
20°
40°
60°
γ
$\frac{E_I}{(\hbar^2/2\mathcal{I}_0)}$
8_1^+
6_1^+
4_2^+
4_1^+
3_1^+
2_2^+
2_1^+
0_1^+
XBL7410-4344

Fig. 2

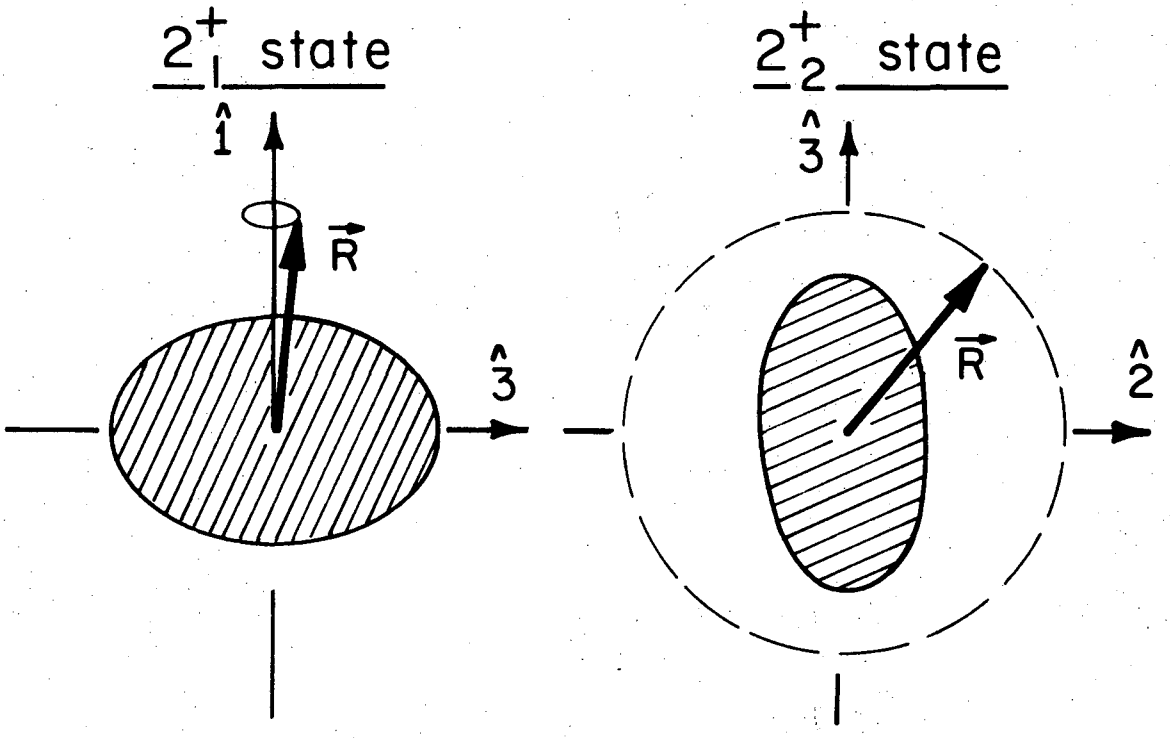

XBL7411-4598

Fig. 3

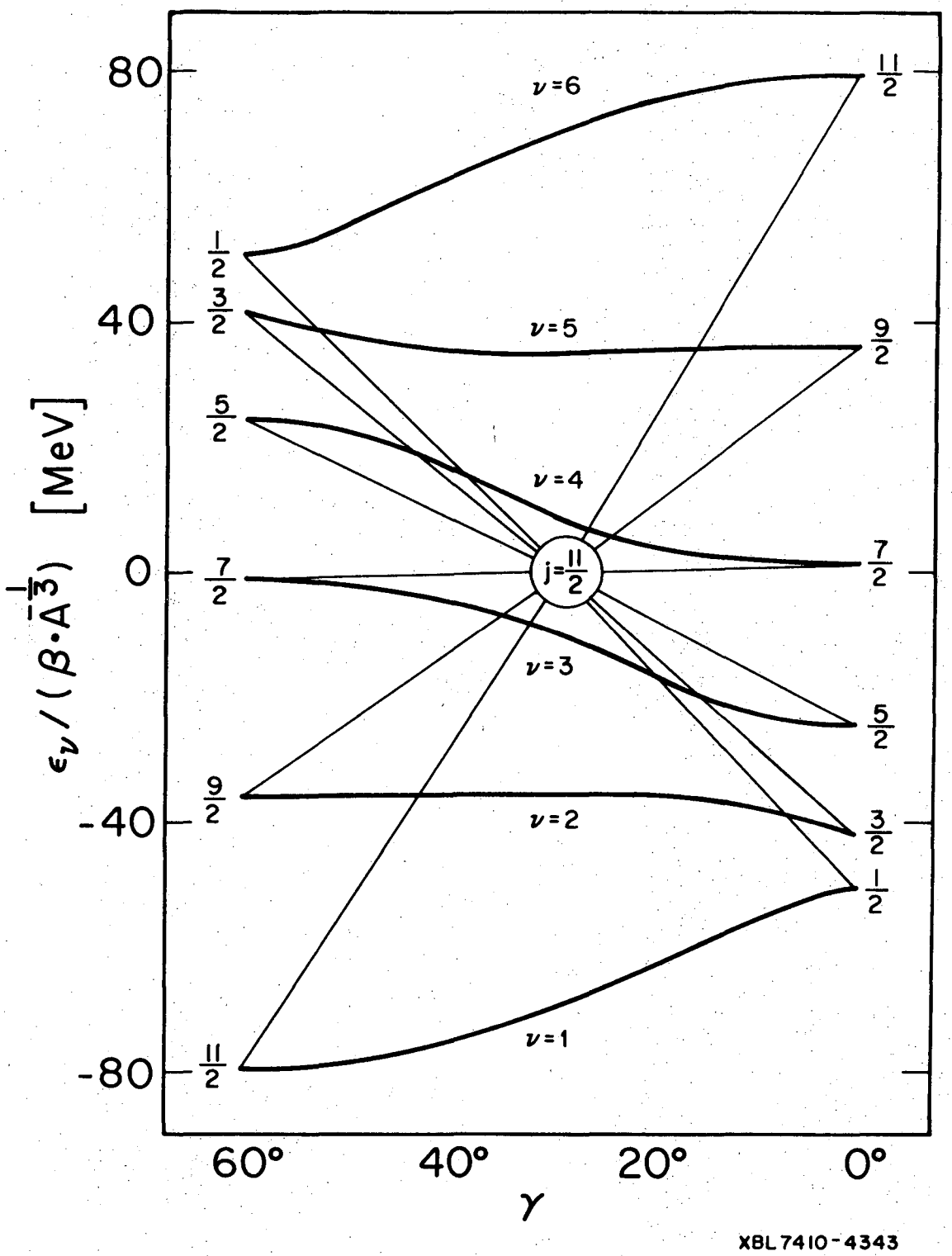
80
40
0
-40
-80
$\epsilon_\nu / (\beta \cdot A^{-\frac{1}{3}})$ [MeV]
$\nu=6$
$\nu=5$
$\nu=4$
$\nu=3$
$\nu=2$
$\nu=1$
$j=\frac{11}{2}$
$\frac{1}{2}$
$\frac{3}{2}$
$\frac{5}{2}$
$\frac{7}{2}$
$\frac{9}{2}$
$\frac{11}{2}$
60°
40°
20°
0°
γ
XBL7410-4343

Fig. 4

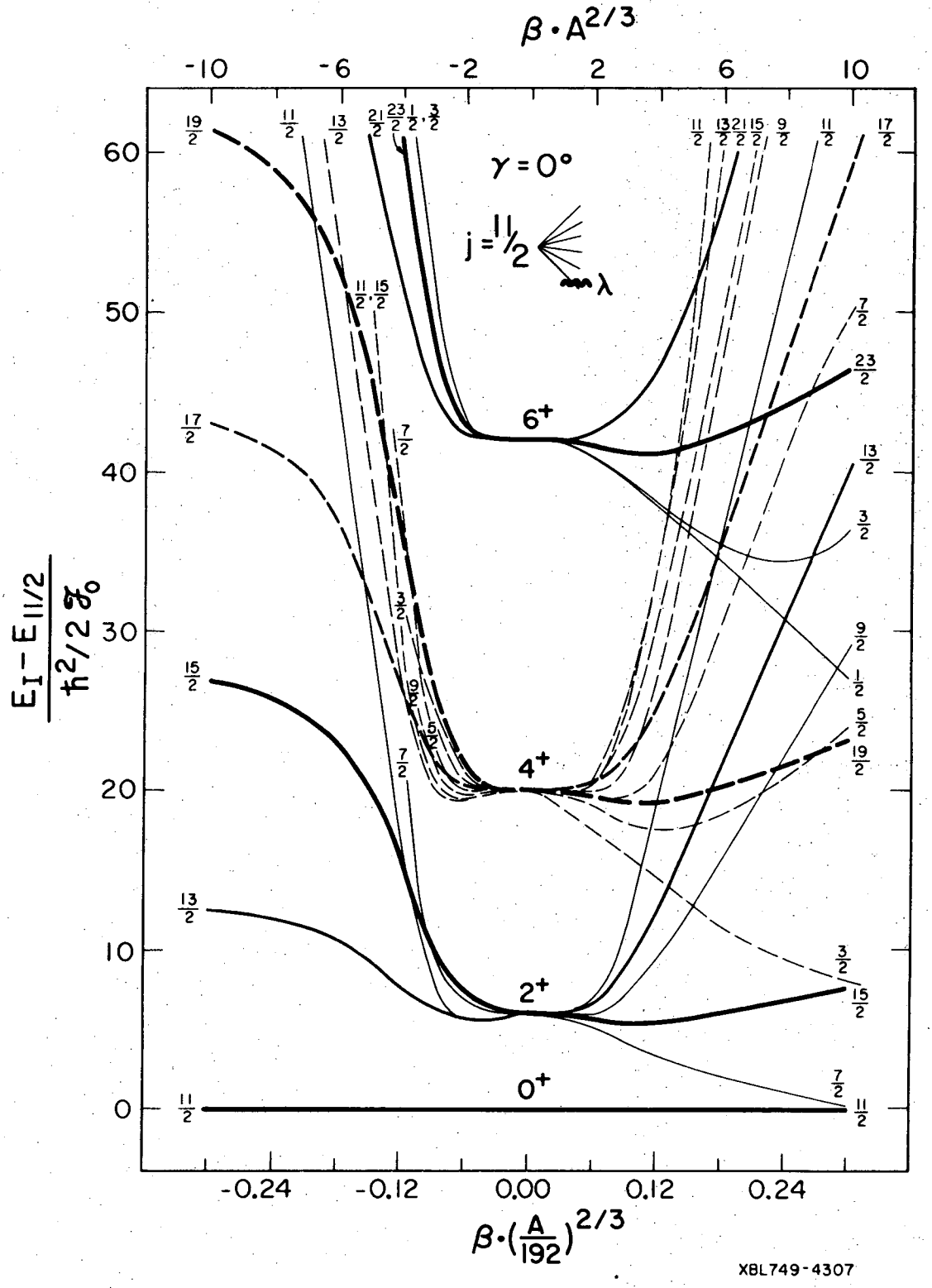
β·A^2/3
-10
-6
-2
2
6
10
γ = 0°
j = 11/2
λ
6+
4+
2+
0+
60
50
40
30
20
10
0
(E_I − E_11/2) / ħ²/2ℑ₀
-0.24
-0.12
0.00
0.12
0.24
β·(A/192)^2/3
XBL749-4307

Fig. 5a

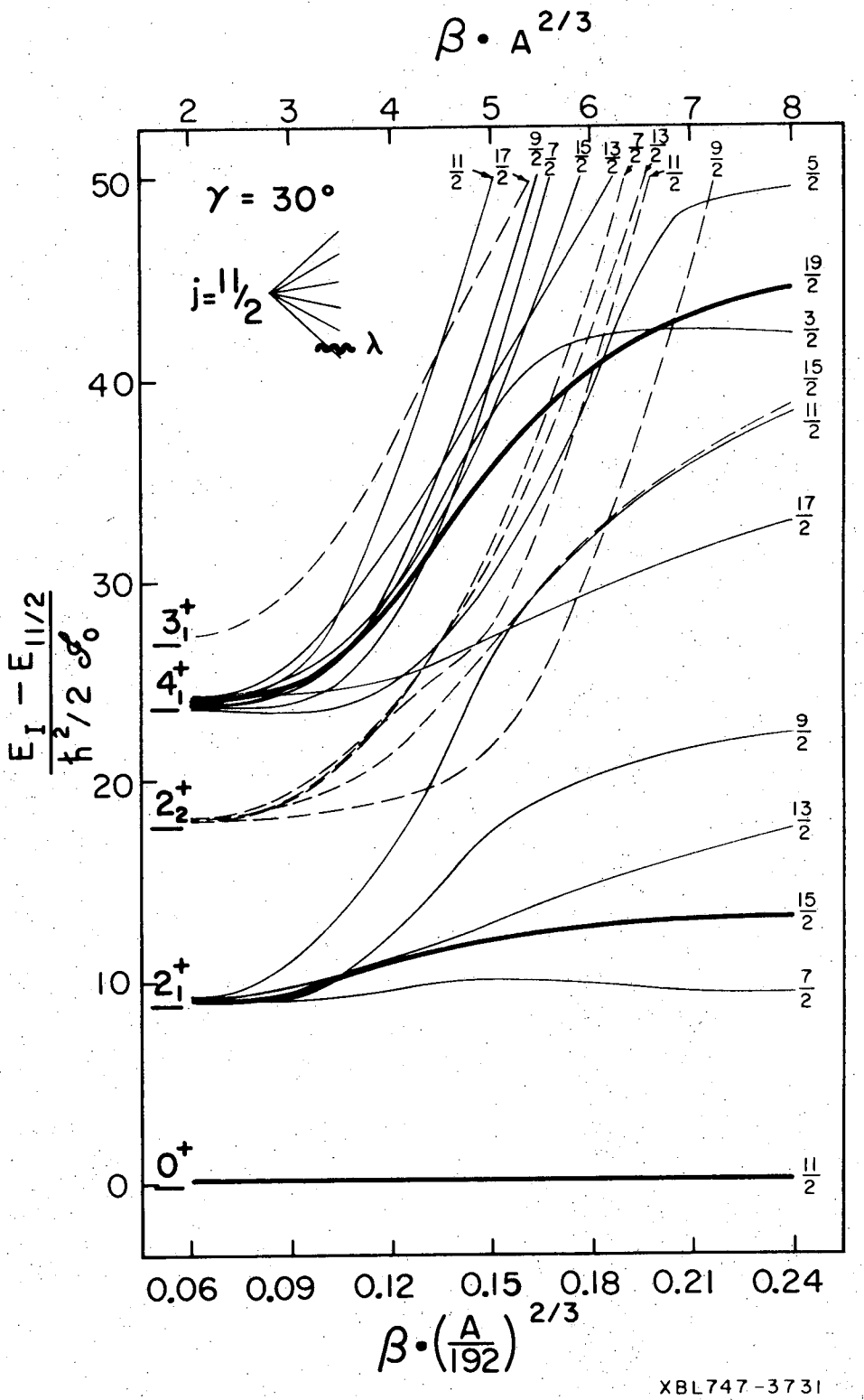
β • A^2/3
2
3
4
5
6
7
8
50
40
30
20
10
0
γ = 30°
j=11/2
λ
11/2
17/2
9/2
7/2
15/2
13/2
7/2
13/2
11/2
9/2
5/2
19/2
3/2
15/2
11/2
17/2
9/2
13/2
15/2
7/2
11/2
3⁺1
4⁺1
2⁺2
2⁺1
0⁺
(E_I − E_11/2) / (ħ²/2 ℐ₀)
0.06
0.09
0.12
0.15
0.18
0.21
0.24
β • (A/192)^2/3
XBL747-3731

Fig. 5b

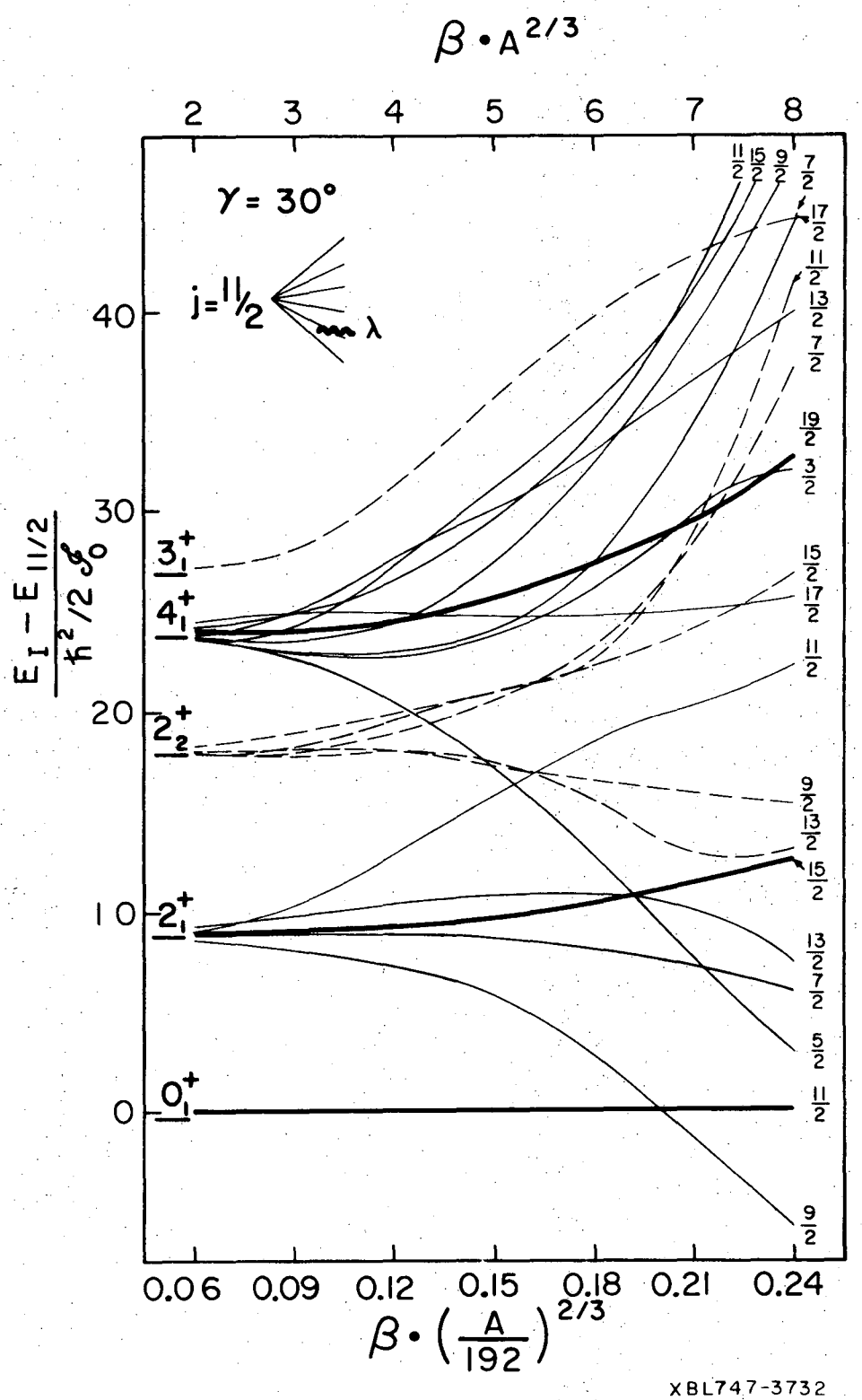
β • A^2/3
2
3
4
5
6
7
8
γ = 30°
j = 11/2
λ
40
30
20
10
0
3+1
4+1
2+2
2+1
0+1
E_I − E_11/2 / ħ²/2ℐ₀
0.06
0.09
0.12
0.15
0.18
0.21
0.24
β • (A/192)^2/3
XBL747-3732

Fig. 5c

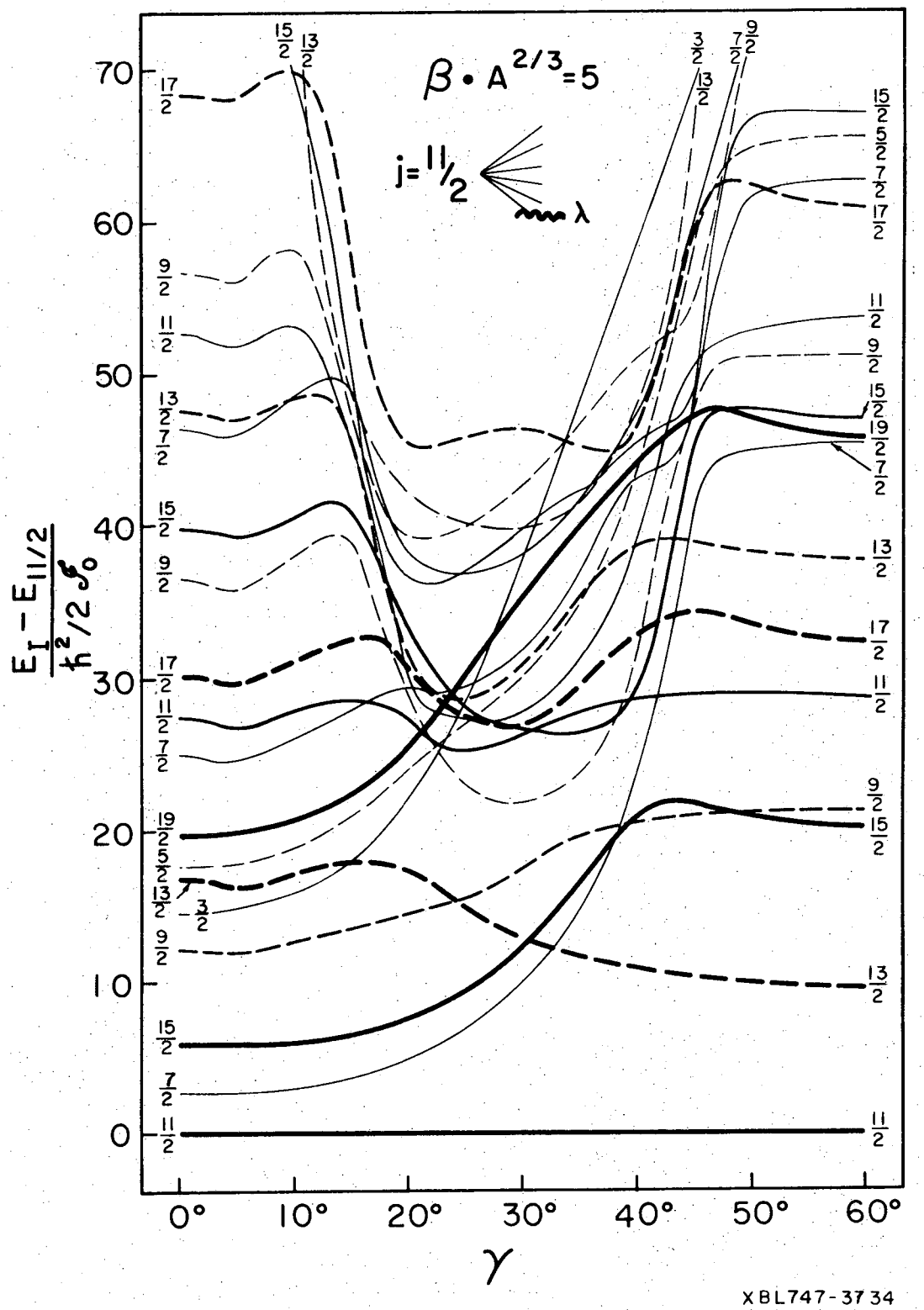
$\beta \cdot A^{2/3} = 5$
$j = 11/2$
λ
$\frac{E_I - E_{11/2}}{\hbar^2/2\mathcal{J}_0}$
γ
0°
10°
20°
30°
40°
50°
60°
0
10
20
30
40
50
60
70
XBL747-3734

Fig. 6a

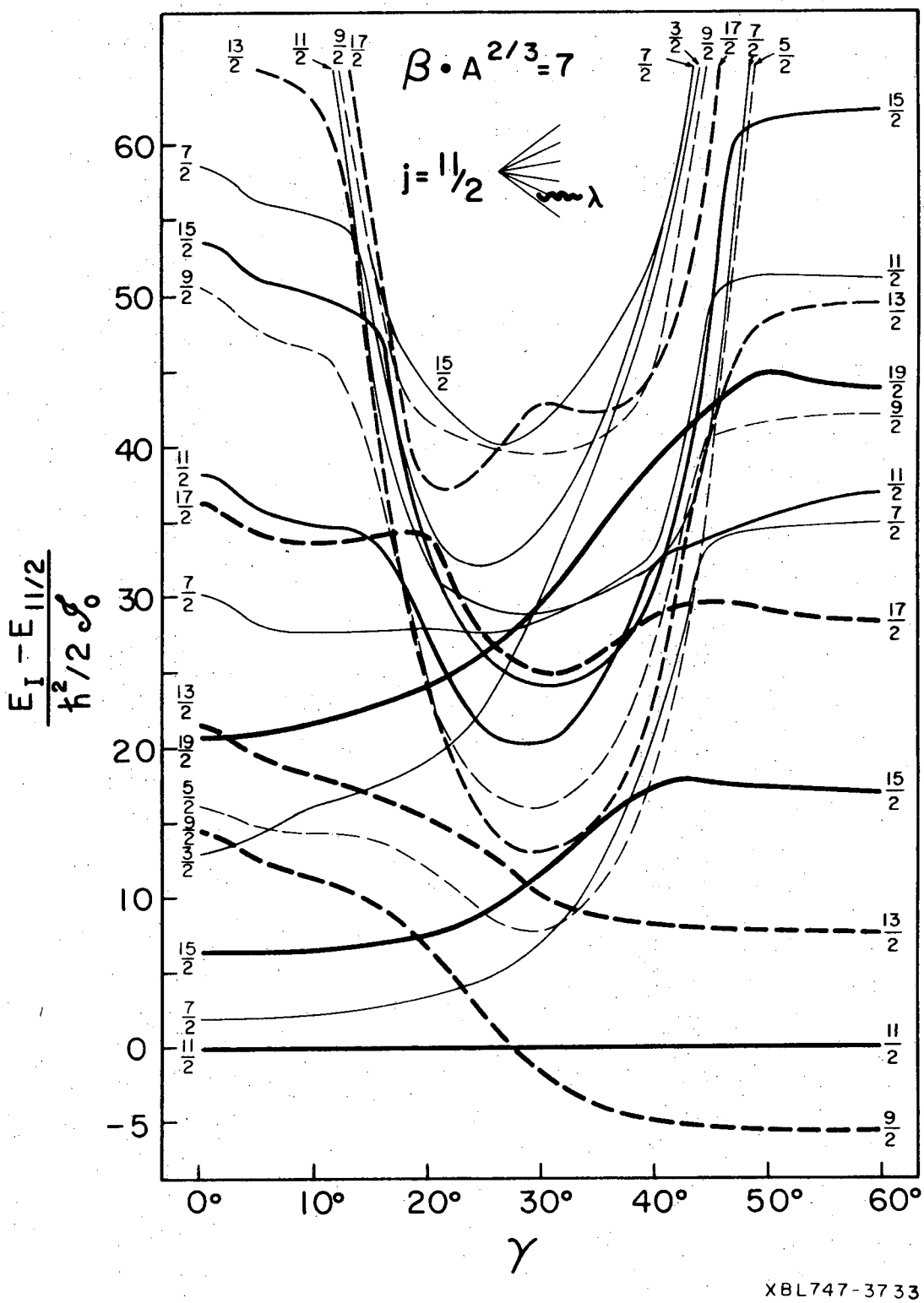
$\beta \cdot A^{2/3} = 7$
$j = 11/2$
λ
$\frac{E_I - E_{11/2}}{\hbar^2/2\mathcal{J}_0}$
γ
0°
10°
20°
30°
40°
50°
60°
60
50
40
30
20
10
0
-5
XBL747-3733

Fig. 6b

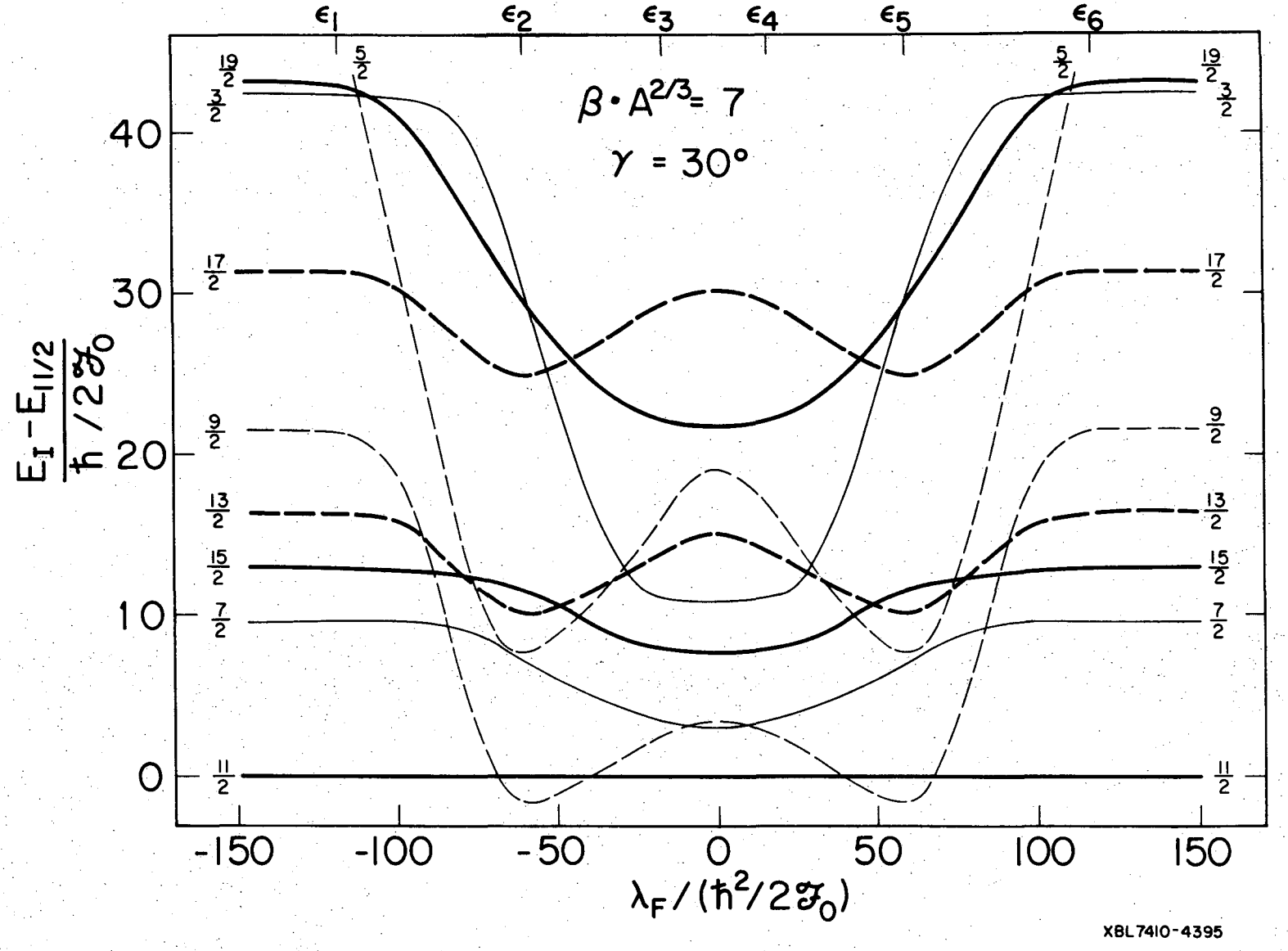
ϵ_1 ϵ_2 ϵ_3 ϵ_4 ϵ_5 ϵ_6
$\beta \cdot A^{2/3} = 7$
$\gamma = 30°$
$\frac{E_I - E_{11/2}}{\hbar/2\mathcal{J}_0}$
40
30
20
10
0
$\frac{19}{2}$ $\frac{5}{2}$ $\frac{3}{2}$ $\frac{17}{2}$ $\frac{9}{2}$ $\frac{13}{2}$ $\frac{15}{2}$ $\frac{7}{2}$ $\frac{11}{2}$
-150 -100 -50 0 50 100 150
$\lambda_F / (\hbar^2/2\mathcal{J}_0)$
XBL7410-4395

Fig. 7

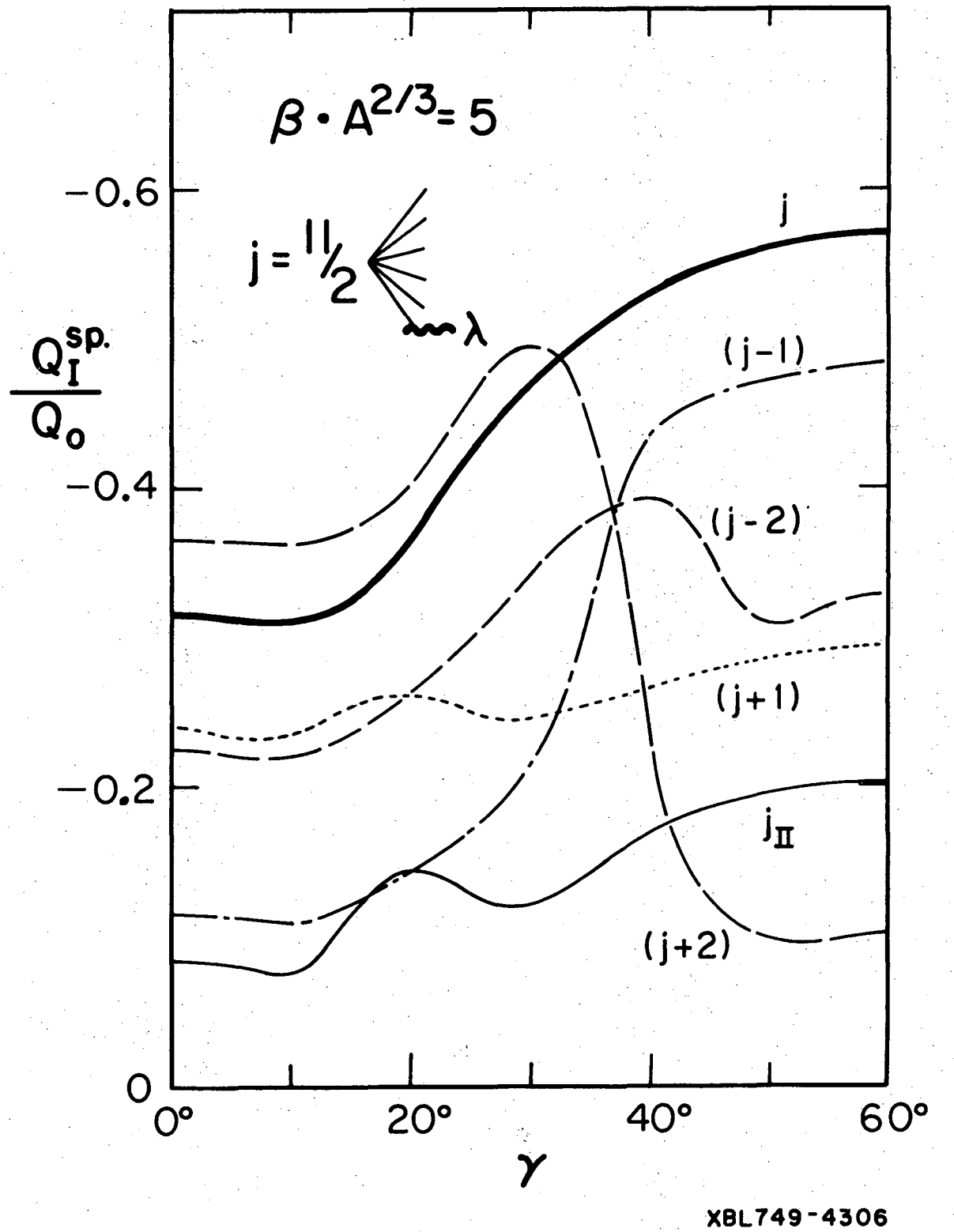
$\beta \cdot A^{2/3} = 5$
$j = 11/2$
λ
j
(j-1)
(j-2)
(j+1)
j_{II}
(j+2)
$\frac{Q_I^{sp.}}{Q_o}$
-0.6
-0.4
-0.2
0
0°
20°
40°
60°
γ
XBL749-4306

Fig. 8

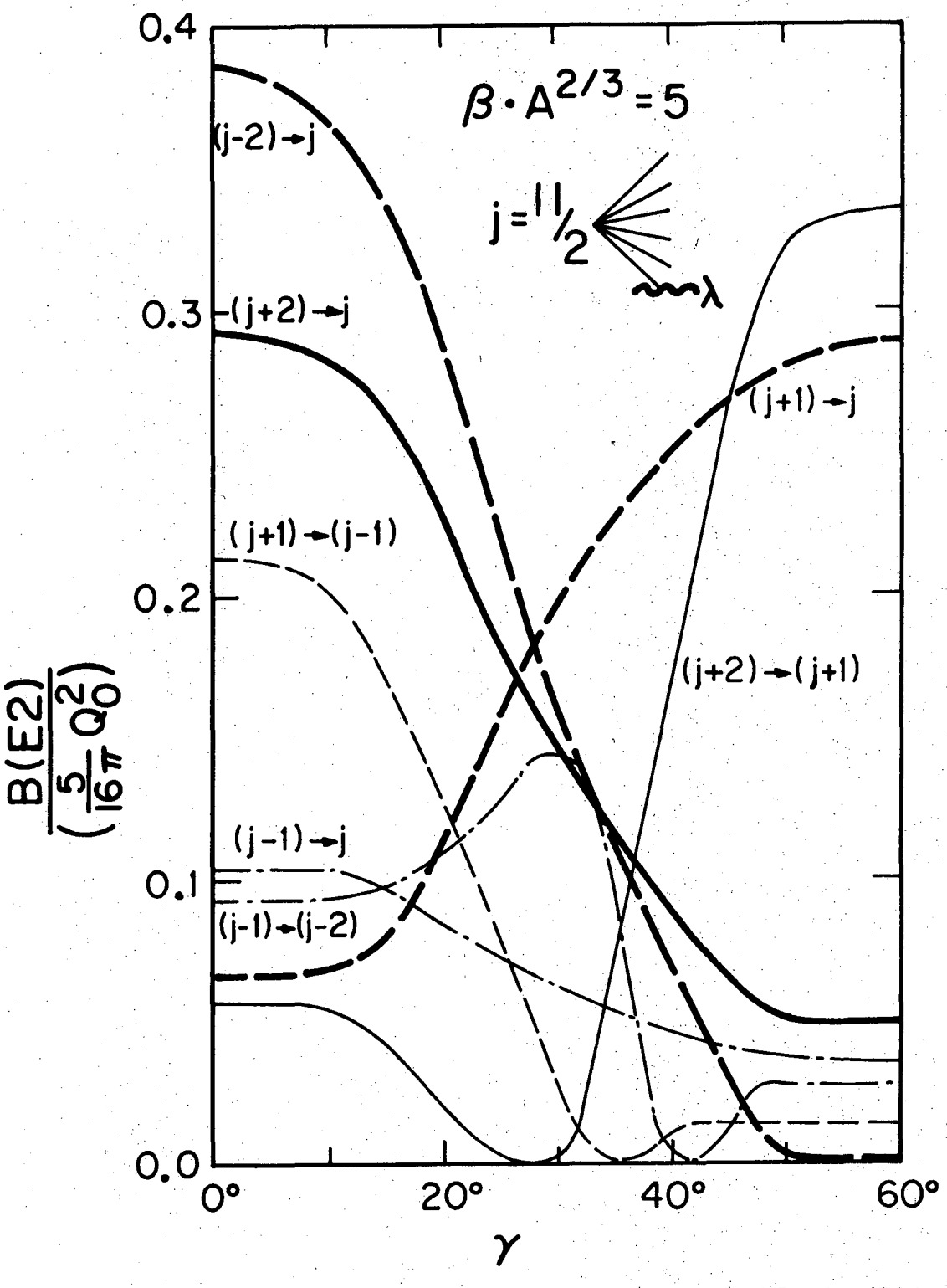
0.4
0.3
0.2
0.1
0.0
0°
20°
40°
60°
γ
$\frac{B(E2)}{(\frac{5}{16\pi}Q_0^2)}$
$\beta \cdot A^{2/3} = 5$
$j = 11/2$
(j-2)→j
(j+2)→j
(j+1)→j
(j+1)→(j-1)
(j+2)→(j+1)
(j-1)→j
(j-1)→(j-2)
XBL 749-4304

Fig. 9

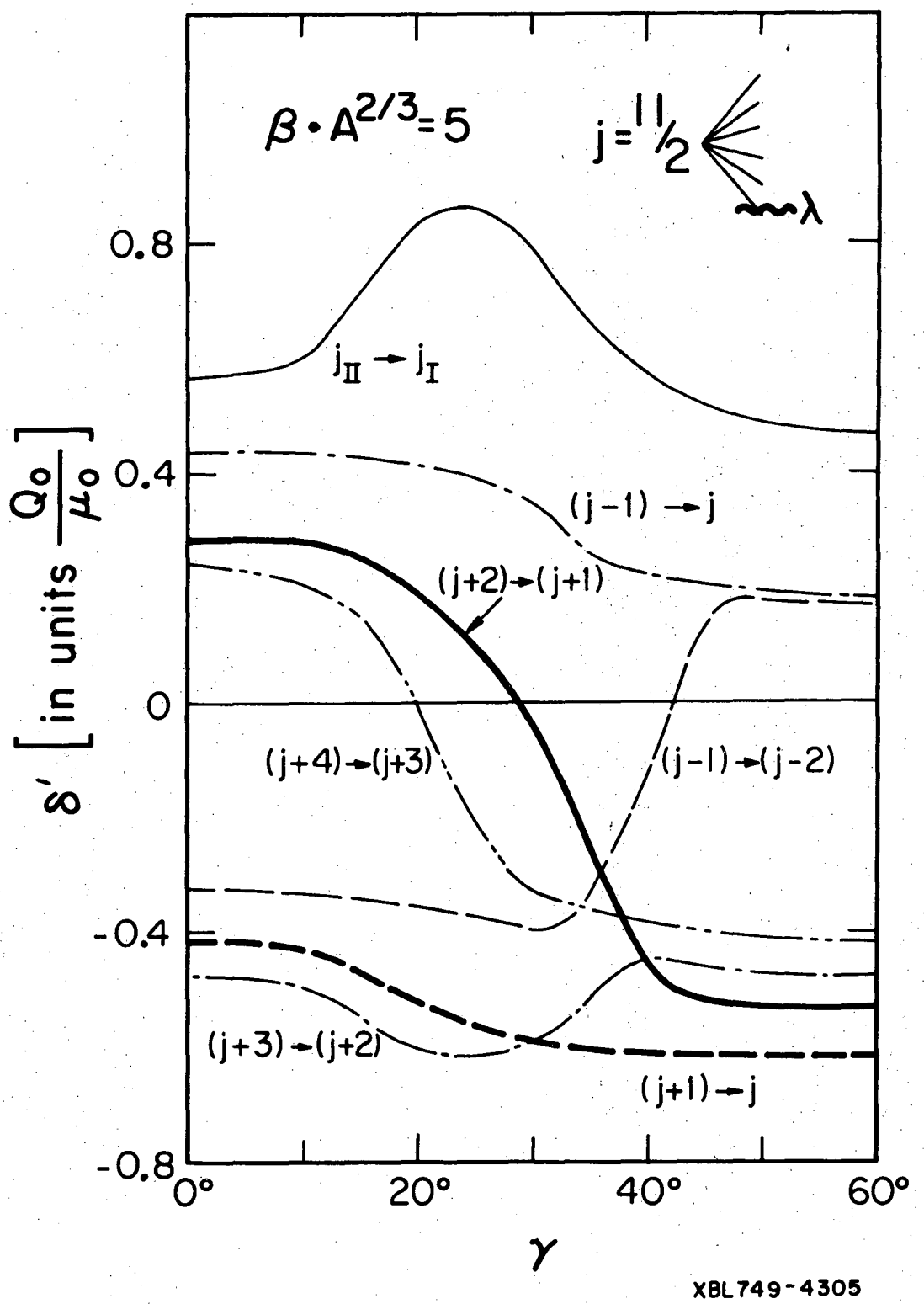
$\beta \cdot A^{2/3} = 5$
$j = 11/2$
λ
0.8
0.4
0
-0.4
-0.8
$j_{II} \rightarrow j_I$
$(j-1) \rightarrow j$
$(j+2) \rightarrow (j+1)$
$(j+4) \rightarrow (j+3)$
$(j-1) \rightarrow (j-2)$
$(j+3) \rightarrow (j+2)$
$(j+1) \rightarrow j$
δ' [in units $\frac{Q_0}{\mu_0}$]
0°
20°
40°
60°
γ
XBL749-4305

Fig. 10

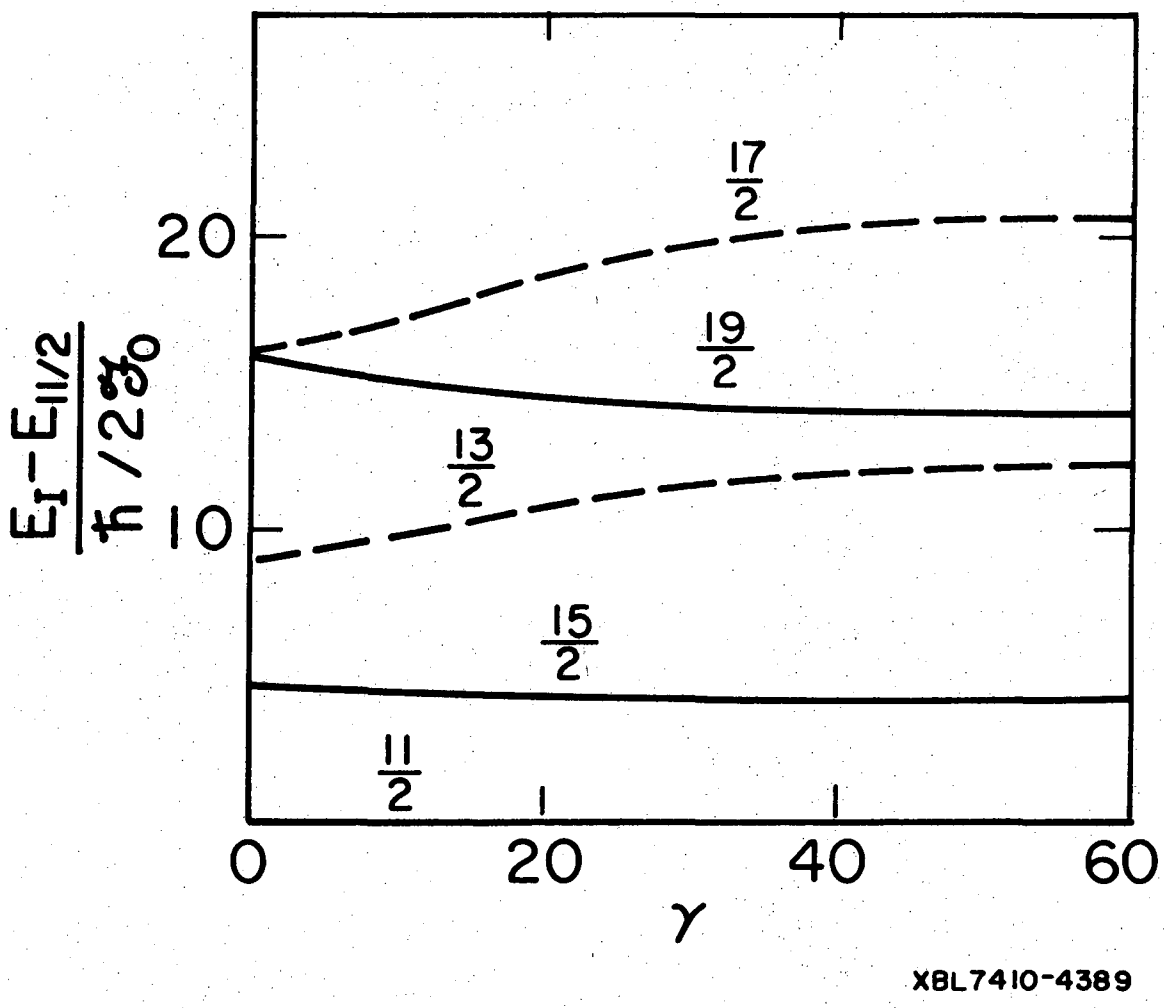
$\frac{E_I - E_{11/2}}{\hbar/2\mathcal{J}_0}$
20
10
0
20
40
60
γ
17/2
19/2
13/2
15/2
11/2
XBL7410-4389

Fig. 11

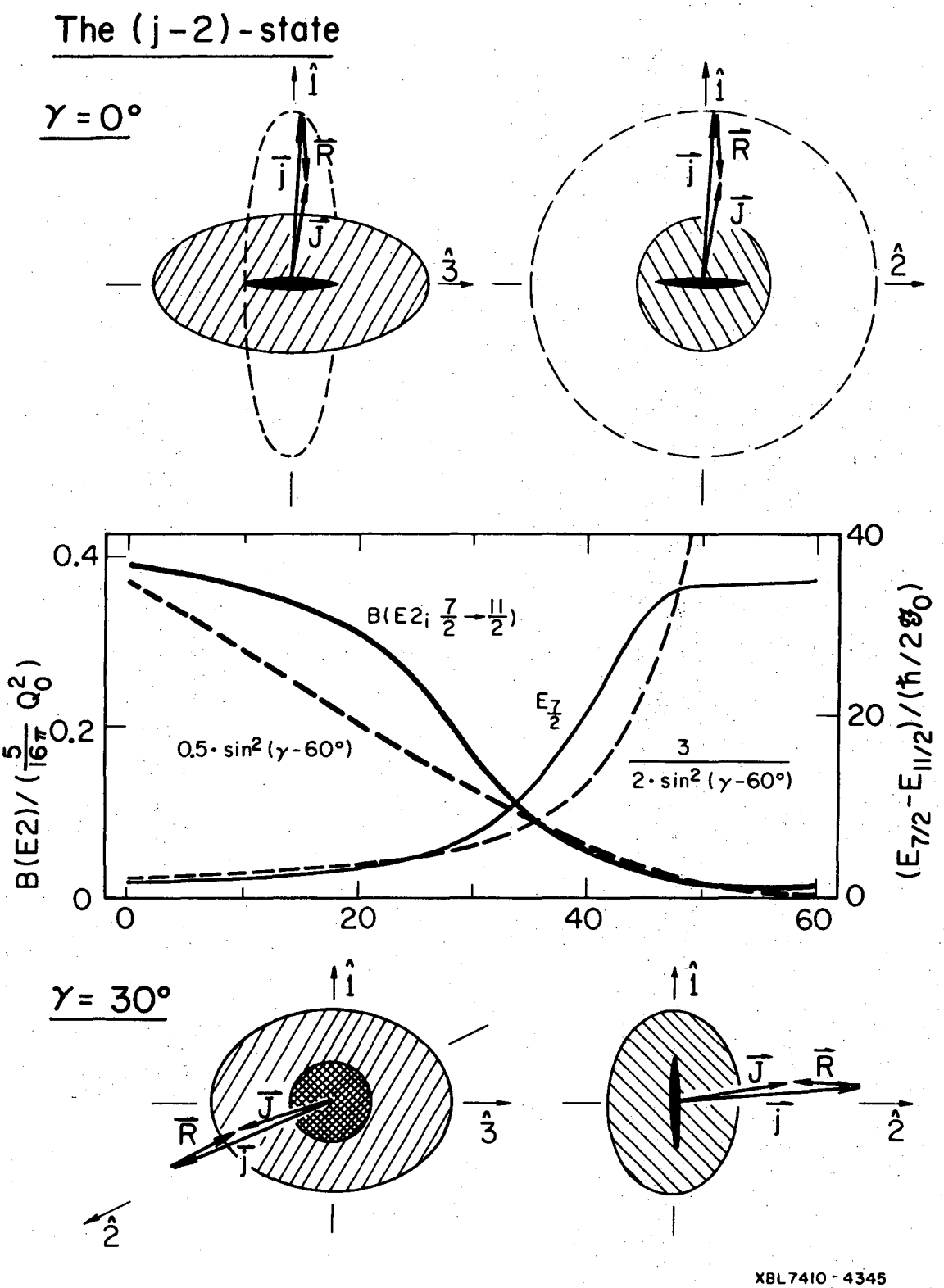
The (j−2)-state
γ = 0°
γ = 30°
B(E2i 7/2 → 11/2)
E7/2
0.5 · sin²(γ−60°)
3 / 2 · sin²(γ−60°)
B(E2) / (5/16π Q0²)
(E7/2 − E11/2) / (ħ/2ω0)
XBL7410-4345

Fig. 12

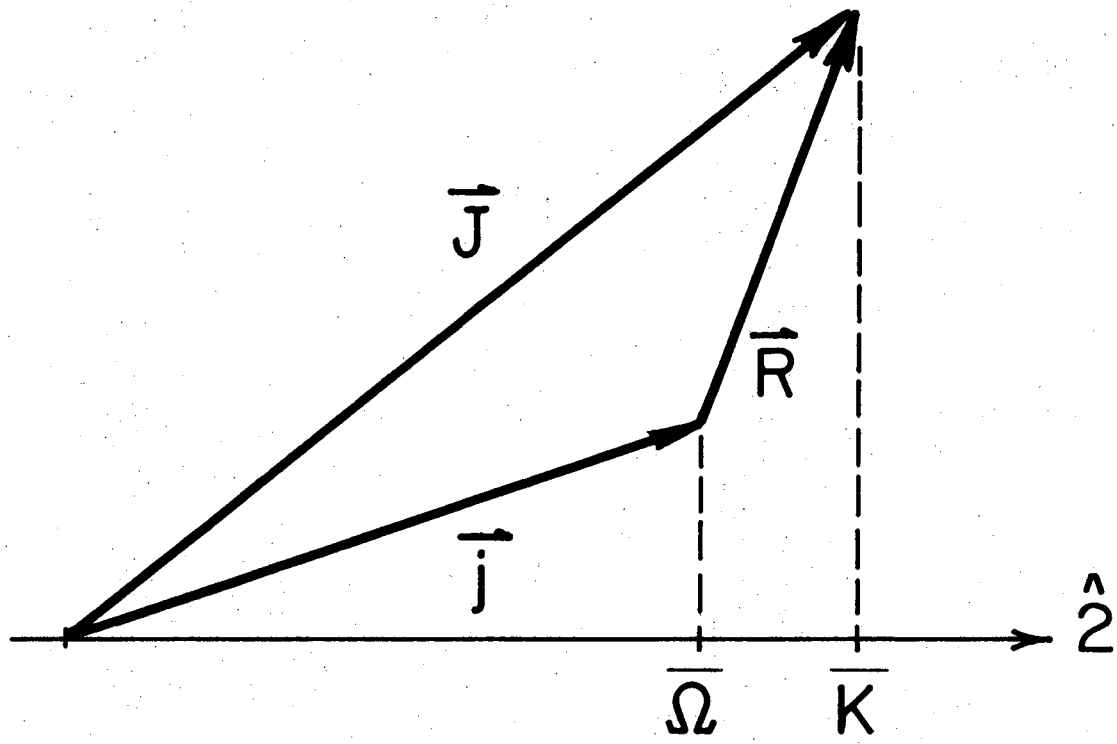

XBL7410-4391

Fig. 13

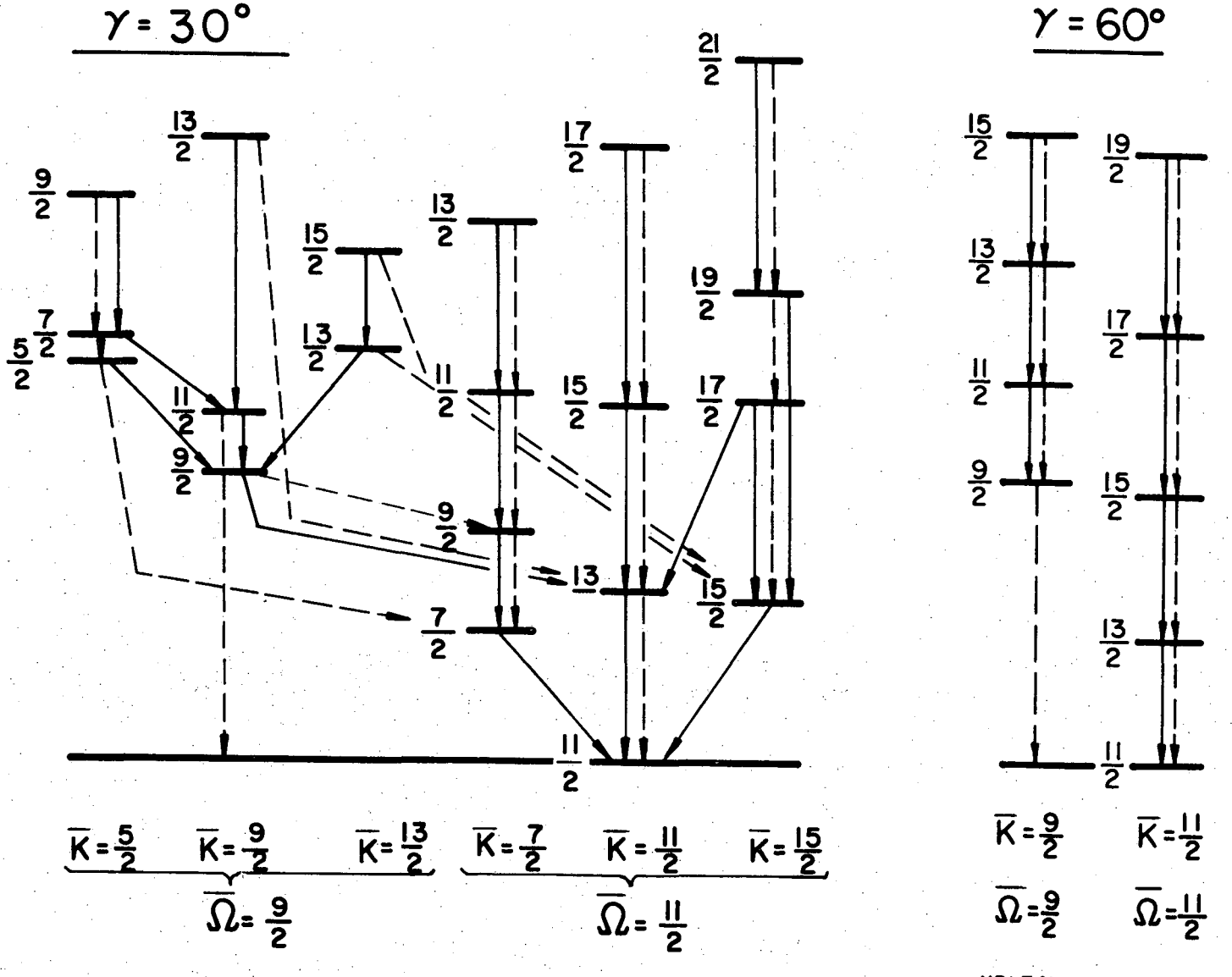

Fig. 14

TECHNICAL INFORMATION DIVISION
LAWRENCE BERKELEY LABORATORY
UNIVERSITY OF CALIFORNIA
BERKELEY, CALIFORNIA 94720